Tree microbiomes and methane emissions in upland forests

Jonathan Gewirtzman[1†*], Wyatt Arnold[2†], Meghan Taylor[1,3], Hannah Burrows[5], Carter Merenstein[4], David Woodbury[1], Naomi Whitlock[6], Kendall Kraut[6], Leslie Gonzalez[7], Craig R. Brodersen[1,8], Marlyse Duguid[1,8], Peter A. Raymond[1,9], Jordan Peccia[2], Mark A. Bradford[1,8]

[1] Yale School of the Environment, Yale University, New Haven, CT, USA
[2] Department of Chemical and Environmental Engineering, School of Engineering and Applied Science, Yale University, New Haven, CT, USA
[3] WCRP Climate and the Cryosphere, University of Massachusetts, Amherst, Amherst, MA, USA
[4] Harvard College, Harvard University, Boston, MA, USA
[5] Harvard T.H. Chan School of Public Health, Boston, MA, USA
[6] Wesleyan University, Middletown, CT, USA
[7] Yale College, Yale University, New Haven, CT, 06511
[8] The Forest School, Yale School of the Environment, Yale University, New Haven, CT, USA
[9] Yale Center for Natural Carbon Capture, Yale University, New Haven, CT, USA
[†] Contributed equally to this work
* Corresponding author: jonathan.gewirtzman@yale.edu

Summary

- **Rationale**: Trees emit methane and harbor methanogens, but the generality, distribution, and ecosystem significance of these associations remain unclear. We investigated methanogenic colonization across 16 upland forest tree species and evaluated relationships between microbial communities and emissions.
- **Methods**: We measured 1,148 stem fluxes and 276 soil fluxes, quantified methanogens and methanotrophs via droplet digital PCR in 564 samples, characterized communities through 16S rRNA sequencing, and developed models to upscale fluxes ecosystem-wide.
- **Key results**: Methanogens were detected in 97% of heartwood samples (up to 10^7 copies g^{-1}), exceeding mean soil abundances by ~2 orders of magnitude. Wood harbored distinct methanogenic communities (Methanobacteriaceae, Methanomassiliicoccaceae) compared to soils. Individual tree-level gene-flux correlations were weak, reflecting spatial heterogeneity and complex metabolism and transport interactions. However, aggregated tree species-level methanogen:methanotroph ratios correlated significantly with emissions ($R^2 = 0.54$), with methanogen abundance alone explaining 40% of variation.
- **Main conclusion**: Methanogens are common in tree microbiomes across diverse species, concentrated in heartwood with substantial individual variation. Species-level abundance patterns partially explain emission variability, establishing internal production as a widespread contributor to upland tree fluxes. Future multi-omics approaches could strengthen abundance-flux relationships, while resolving ecosystem-scale flux magnitude requires improved quantification of canopy surface area and flux variability.

Keywords: forest carbon cycle; greenhouse gas; heartwood; methanogen; methanotroph; methane emissions; temperate forest; tree microbiome

Introduction

Forests are key regulators of the global methane (CH_4) cycle, functioning as both sinks and sources of this potent greenhouse gas. Methane contributes significantly to climate change, possessing a global warming potential more than 80 times greater than carbon dioxide (CO_2) over a 20-year period (Wood et al. 2023; Forster et al. 2021). While the role of soil in forest methane cycling has been extensively studied, emerging evidence reveals that trees themselves play an active role in methane fluxes (Barba et al., 2019; Gauci, 2025). Tree stems have been identified as both methane emitters and sinks, suggesting that they may also be important regulators of methane dynamics in forest ecosystems. However, the biological and ecological mechanisms underlying these tree-mediated methane fluxes remain poorly understood.

Tree methane emissions may originate from methanogens (methane-producing archaea) and be moderated by methanotrophs (methane-oxidizing bacteria) within tree tissues. Methanogens– microbes which generate methane from hydrogenotrophic, acetoclastic, or methylotrophic methanogenesis, generally in anaerobic environments (Le Mer & Roger 2001)– have been detected in heartwood of multiple species (Zeikus & Ward 1974; Zeikus & Henning 1975; Covey et al. 2012; Yip et al. 2019; Flanagan et al. 2021; Feng et al. 2022; Moisan et al. 2025; Harada et al. 2024; Mochidome et al. 2025). Anaerobic conditions in heartwood (Schink & Ward 1984; Shigo & Hillis 1973; Jensen 1967; Arnold and Gewirtzman et al. 2025), where oxygen diffusion is restricted, may create suitable methanogenic niches (Uroz et al. 2016; Mieszkin et al. 2021), but the extent of colonization, the metabolic pathways, and the overall contribution to forest methane budgets remain unclear (Putkinen et al. 2021; Barba et al. 2024; Barba, Bradford, et al. 2019).

Methanotrophs oxidize CH_4 to CO_2, generally under aerobic conditions. Detected in sapwood and bark, they may mitigate emissions before atmospheric release (Leung et al. 2024; Jeffrey et al. 2021; Carmichael et al. 2024; Gauci et al. 2024). The co-occurrence of methane producers and consumers suggests complex interactions influencing net fluxes at tree and ecosystem scales, but quantitative data on their abundance, activity, and spatial distribution remain sparse (Putkinen et al. 2021). It remains unclear whether methanotroph activity varies with tree species, physiological traits, or environmental conditions.

Tree-mediated methane emissions vary considerably across species, landscapes, and temporal scales. In wetland forests, trees primarily act as conduits for soil-derived methane, transporting CH_4 from anaerobic soils through vascular pathways (Pangala et al. 2013; Pangala et al. 2015; Pangala et al. 2017; Pitz et al. 2018; Jeffrey et al. 2023; Jeffrey et al. 2019). Conversely, upland forests, where well-drained soils are traditionally methane sinks, also have trees that emit methane (Machacova et al. 2023; Bréchet et al. 2025; Hettwer et al. 2025; Pitz & Megonigal 2017; Warner et al. 2017; Covey & Megonigal 2019), suggesting internal production rather than soil transport (Pitz & Megonigal 2017). While a number of recent detections of endophytic methanogens support this hypothesis, factors governing production including tree species, wood chemistry, and microbial interactions remain poorly understood.

The taxonomic, spatial, and environmental distribution of microbial methane producers and consumers within trees remains unresolved. Methanogens are thought to primarily associate with heartwood, but their presence in sapwood or bark lacks systematic investigation (Arnold et al. 2024; Arnold and Gewirtzman et al. 2025). Methanotroph activity in sapwood and bark likely varies with oxygen availability, the presence of alternative electron acceptors, and stem water content (Putkinen et al. 2021). Environmental factors including soil moisture, nutrients, and rhizosphere composition influence methane dynamics, though their interaction with tree-mediated fluxes is unclear (Epron et al. 2022). Climate and tree-specific traits such as wood density and anatomical features, including decay or damage, may regulate microbial colonization and flux potential (Barba, Bradford, et al. 2019).

The ecological and biogeochemical significance of tree-mediated methane emissions extends beyond individual trees to entire forest ecosystems and the planet. Given that forests represent a substantial component of the global methane budget, even small changes in tree methane emissions could have significant implications for atmospheric CH_4 concentrations. The recognition that trees in upland forests may contribute to net methane fluxes challenges traditional assumptions about forest methane cycling and highlights the need for a more integrative approach to forest methane budgets (Gauci 2025).

Study Objectives

Despite growing evidence of tree methane emissions, the underlying microbial and physiological mechanisms remain poorly characterized, particularly in upland forests where soils consume atmospheric methane. We investigated methane fluxes and associated microbial communities across a moisture gradient from upland to transitional wetland sites at a mixed temperate forest in Connecticut, USA, addressing four objectives:

(1) Quantify tree methane emissions across environmental gradients. We quantified methane fluxes from stems and soils across upland, intermediate, and transitional wetland sites, examining vertical profiles to differentiate soil-derived transport from internal production. We hypothesized upland trees would show uniform vertical profiles consistent with internal production, contrasting with exponential height-dependent decline in wetland trees. We assessed species-specific differences and performed variance partitioning to identify emission drivers.

(2) Characterize methanogenic communities within trees. We determined methanogen abundance and distribution across heartwood and sapwood using droplet digital PCR and characterized taxonomic composition via 16S rRNA sequencing. We tested whether tree methanogens represent distinct communities from soil populations, hypothesizing heartwood would harbor higher abundances due to lower oxygen. Through co-occurrence analysis and functional inference, we characterized microbial consortia and metabolic pathways, predicting fermentative bacteria would co-occur with methanogens to provide substrates.

(3) Establish microbial gene abundance-flux relationships. We examined whether methanogen and methanotroph populations correlate with emission rates at both individual tree

and species levels. We tested correlations at multiple scales to determine whether aggregation across individuals would reduce noise from spatial heterogeneity and reveal underlying biological relationships between microbial abundance and methane flux.

(4) Evaluate ecosystem-scale impacts. Using random forest models incorporating tree characteristics and environmental drivers, we upscaled measurements to estimate forest-wide fluxes. We calculated how tree emissions offset soil consumption to determine whether tree fluxes meaningfully alter upland forest methane sink status.

Here we present 1,148 tree stem flux measurements from 482 individual trees across 16 species; 276 soil flux measurements; and molecular quantification of methanogens and methanotrophs from 564 tree and soil samples collected across upland to transitional wetland gradients in a temperate mixed forest. Through integrated flux measurements, molecular quantification, and community analysis, we aimed to establish whether methanogens are endemic tree microbiome components and determine their contribution to emissions across species and environmental gradients. This multi-scale approach addresses fundamental questions about the origin, regulation, and magnitude of tree-mediated methane emissions, advancing mechanistic understanding of this emerging component of the global methane cycle.

Materials and Methods

Study site

Field measurements were conducted at Yale-Myers Forest, a 3,213-ha research forest in northeastern Connecticut, USA (41°56′N, 72°07′W). The forest comprises second-growth mixed-deciduous vegetation established on abandoned agricultural land since the mid-19th century, with elevations ranging from 170-300 m a.s.l. The climate is temperate and humid with mean annual temperature of 9.5°C (summer: 21°C, winter: -2°C) and 123 cm annual precipitation. Soils consist of glacial till-derived, moderately to well-drained stony loams overlaying bedrock.

Measurements during 2020-2021 and 2023 were conducted within an 8-ha permanent forest inventory plot established following standardized protocols, with some additional 2020-2021 measurements in transitional wetland immediately adjacent to the plot. Destructive sampling for microbiome analysis (2021-2022) occurred in nearby forest stands of similar composition and developmental history, as destructive sampling was prohibited within the long-term monitoring plot.

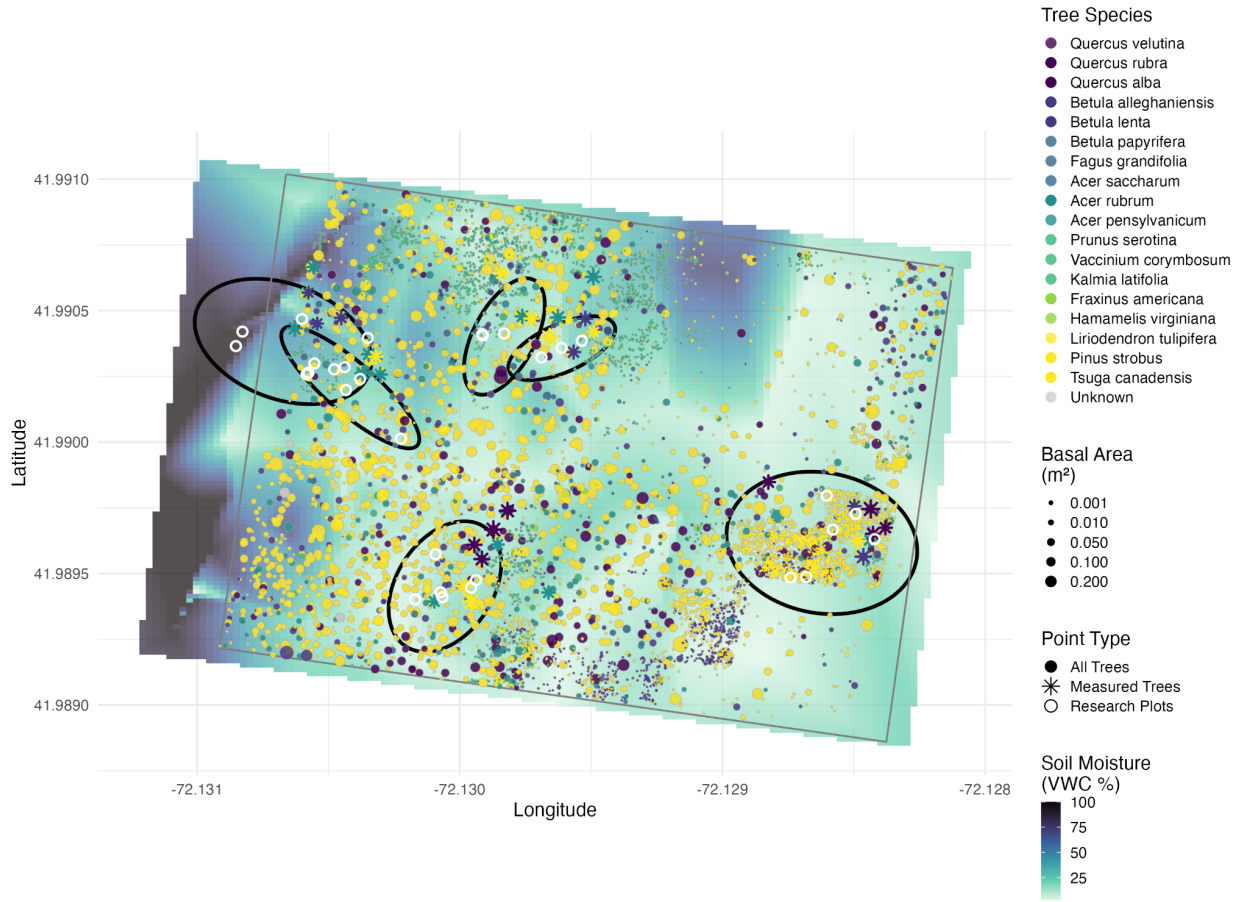

Tree stem methane flux measurements

Chamber designs

Two chamber types were employed for stem flux measurements. Semi-rigid chambers (2020-2021) were constructed following (Siegenthaler et al. 2016) using transparent polyethylene terephthalate (PET) sheets . Sheets were framed with 1.5 cm thick × 3 cm wide adhesive-backed expanded neoprene strips for gas-tight sealing, with two vertical neoprene wedges maintaining equidistant spacing from the stem. Chamber volume was calculated as: $Vc = (HL/(Dstem + 2T)) \times [(Dstem + 2T)/2]^2 - [Dstem/2]^2 - Vwedges$, where H = height, L = periphery length, Dstem = stem diameter, and T = chamber thickness. Chambers were wrapped around stems, secured with ratchet straps, and gaps sealed with modeling clay tested to confirm no CH_4 or CO_2 off-gassing.

Rigid chambers (2021-2023) were constructed from transparent plastic containers (Rubbermaid) with arcs cut to fit tree stems. Chamber volumes (0.5-2.0 L) were determined by gas standard dilution in the laboratory (Jeffrey et al., 2020; Siegenthaler et al., 2016). Enclosed surface area was calculated as the product of the chamber's planar area and arc length. Chambers were sealed with potting clay (Amaco) and secured with lashing straps. Seal integrity was verified through

visual inspection, blowing on perimeter to check for spikes in CO_2, and confirmed by monitoring concentration linearity.

Measurement protocol

All chambers were connected via 5-mm internal diameter PVC tubing (Bev-a-Line) to a portable off-axis integrated cavity output spectroscopy analyzer (GLA131-GGA, Los Gatos Research) measuring CO_2, CH_4, and H_2O concentrations at 1 Hz with CH_4 precision <0.9 ppb. The analyzer's 5 L min^{-1} flow rate allowed complete chamber volume turnover within ~30 s. Measurements lasted 3-10 min per location, with the initial 30 s excluded for equilibration.

During the 2020-2021 temporal survey, measurements were collected from 41 trees (21 upland, 10 intermediate, 10 wetland) and 30 soil collars distributed across 6 plots (2 plots per landscape position) during 10 sampling campaigns from June 2020 to May 2021. Soil collars were distributed as follows: upland plots with 12 collars (2 plots × 6 collars), intermediate plots with 6 collars (2 plots × 3 collars), and wetland plots with 12 collar positions (2 plots × 6 collars, measured under both wetland-dry and wetland-saturated conditions). The 2021 intensive survey measured fluxes at three heights (50, 125, 200 cm) on the southern aspect of 158 trees across 16 species: *Acer rubrum*, *A. saccharum*, *Betula alleghaniensis*, *B. lenta*, *B. papyrifera*, *Carya ovata*, *Fagus grandifolia*, *Fraxinus americana*, *Kalmia latifolia*, *Pinus strobus*, *Prunus serotina*, *Quercus alba*, *Q. rubra*, *Q. velutina*, *Sassafras albidum*, and *Tsuga canadensis*. The 2022 vertical profile study measured a single mature *Q. velutina* at seven heights (0.5, 1.25, 2, 4, 6, 8, 10 m), with heights >2 m accessed via arborist climbing equipment. The 2023 survey expanded to 335 trees with measurements standardized at breast height (125 cm).

Soil methane flux and associated measurements

Soil CH_4 fluxes (2020–2021) were measured using static chambers consisting of PVC collars (25 cm diameter) inserted 5 cm into soil at least 24 h before measurement to minimize disturbance. A PVC cap chamber was sealed to collars during measurements using the same analyzer system. Soil moisture was characterized in December 2020 through transects perpendicular to moisture gradients, with volumetric water content measured at 12 cm depth using a handheld sensor (HydroSense, Campbell Scientific). Measurements along transects were collected at a spacing of ~30 m between points, ensuring coverage across both fine-scale and broader soil moisture variability. Soil temperature was recorded at 10 cm depth during flux measurements.

Flux calculations

Methane and CO_2 fluxes were calculated using the goFlux R package v2.0.0 (Rheault et al. 2024), which implements both linear (LM) and non-linear Hutchinson-Mosier (HM) models with automatic water vapor dilution correction (Hutchinson & Mosier 1981; Hüppi et al. 2018). The flux equation:

$$F = (dC/dt) \times (Vc/Ac) \times (P/RT) \times (1 - XH_2O)$$

where F = flux (nmol m^{-2} s^{-1} for CH_4; µmol m^{-2} s^{-1} for CO_2), dC/dt = concentration change rate, Vc = chamber volume (L), Ac = surface area (m^2), P = atmospheric pressure (101.325 kPa), R = 8.314 L kPa K^{-1} mol^{-1}, T = temperature (K), and XH_2O = water vapor mole fraction.

Model selection used the best.flux() function with criteria: goodness-of-fit metrics (MAE, RMSE < instrument precision; AICc), physical constraints (g-factor < 2.0 where g = HM flux/LM flux; $\kappa/\kappa max \leq 1.0$), and quality thresholds ($P < 0.05$; flux > minimal detectable flux; $n \geq 60$ observations). CO_2 flux R^2 served as a chamber seal quality metric, as tree respiration ensures consistently positive CO_2 fluxes.

Internal gas sampling

Tree internal gas concentrations were measured by drilling holes with 5-mm increment borers from bark to pith, then sealing with gas-impermeable tape (2021-2022) or butyl rubber stoppers (2024). After 5 min equilibration, 20 ml gas was extracted using gas-tight syringes (Hamilton) and stored overpressurized in pre-evacuated 12 ml Exetainer vials (Labco). Analysis at Yale Analytical and Stable Isotope Center employed gas chromatography with flame ionization detection for CH_4 and CO_2, and electron capture detection for N_2O and O_2. Calibration used certified standards (0-60,000 ppm CH_4) with ambient air blanks between runs.

Microbiome sampling and processing

Tree cores were collected at 125 cm height using 5.15-mm increment borers (Haglöf Sweden) flame-sterilized between trees. Cores were immediately wrapped in sterile aluminum foil and frozen on dry ice, then stored frozen at -80°C until further analysis. Processing followed methods we optimized and reported (Arnold et al. 2024), and involved: (i) sectioning into operationally-defined heartwood (inner 5 cm from pith) and sapwood (outer 5 cm from bark); (ii) lyophilization for 72 h; (iii) cryogenic grinding (Spex 6775 Freezer/Mill) with 10 min liquid nitrogen pre-cooling followed by two cycles of 2 min grinding and 2 min cooling at 10 cycles s^{-1}, with materials flame-sterilized or bleached between samples.

Soil samples were collected at four cardinal directions around each tree at distances equal to tree circumference or 1 m (whichever greater). Samples were separated by horizon (organic; mineral to 30 cm depth or refusal), composited by horizon, sieved to 4 mm in the field, and immediately frozen on dry ice then stored at -80°C until further analysis.

Molecular analyses

DNA was extracted from 100 mg ground wood or 250 mg soil using MagMAX Microbiome Ultra Nucleic Acid Isolation Kit with KingFisher Apex automated extraction, eluting into 75 µl (wood) or 100 µl (soil). Samples with potential PCR inhibitors were further processed using Zymo OneStep-96 PCR Inhibitor Removal Kit. Microbial communities were characterized through 16S rRNA amplicon sequencing at University of Minnesota Genomics Center following protocols in Arnold and Gewirtzman et al. (2025). The 16S rRNA V4 region was amplified using 515F/806R primers with PNA blockers reducing plant DNA amplification. Sequencing

employed Illumina MiSeq with 2×300 bp paired-end chemistry and dual indexing. Sequencing results from this analysis were also reported in (Arnold and Gewirtzman et al. 2025).

Methanogen (mcrA gene) and methanotroph (pmoA and mmoX genes) abundances were quantified using droplet digital PCR (Bio-Rad QX200), also using methods reported in (Arnold et al. 2024). For mcrA quantification (Steinberg & Regan 2009; Kolb et al. 2003), we used our novel probe-based assay employing FAM-based degenerate primers and probe set (Forward: ACGACYTRCAGGAYCAGTGY, Probe: WGGWCCWAACTAYCCBAACTACG, Reverse: TGGTGWCCBACGTTCATYG) which produces a 118 bp amplicon. This was found to reduce the rate of false positives found in previous methods, and is recommended for environments that may harbor low abundance methanogen populations. Reaction conditions followed the published method: 95°C for 10 min, followed by 40 cycles of 94°C for 30 s and 48°C for 1 min 20 s, then 98°C for 10 min. Reactions used ddPCR Supermix for Probes (No dUTP) (Bio-Rad) with primer concentrations of 900 nM and probe concentration of 250 nM. For pmoA and mmoX genes, EvaGreen chemistry was employed with previously published primers (Luesken et al. 2011; McDonald & Murrell 1997; McDonald et al. 1995). All assays included standards and negative controls. Primers were synthesized at the Keck Oligonucleotide Synthesis facility at Yale University. Probes were synthesized by IDT using their PrimeTime chemistry.

Bioinformatic and statistical analyses

Sequence data were processed using DADA2 (Callahan et al. 2016) via Nephele v2.23.2 (Weber et al. 2018), with taxonomic assignment using SILVA v138.1 (16S) database (Quast et al. 2013). After filtering sequences with <10 reads and removing chloroplast/mitochondrial ASVs, samples were rarefied to 3,500 reads. Community analyses employed phyloseq and microeco R packages using weighted/unweighted UniFrac distances (McMurdie & Holmes 2013; Liu et al. 2021). Functional inference used PICRUSt2 (Douglas et al. 2020) and FAPROTAX (Louca et al. 2016).

Variance partitioning employed linear mixed-effects models in lme4 (Bates et al. 2015) with tree identity as random effect and species, diameter, and moisture as fixed effects. Random Forest models using ranger (Wright & Ziegler 2017) were developed to upscale fluxes using environmental predictors including temperature, moisture, seasonal indices, and taxonomic information, with separate models for stem and soil fluxes.

Results

1. Tree and Soil Methane Fluxes from Upland to Transitional Wetland Sites

Methane flux measurements from both tree stems and soil revealed distinct patterns across upland, intermediate, and transitional wetland environments at Yale-Myers Forest during the 2020-2021 survey period. In upland sites, tree stems consistently showed positive CH_4 fluxes (mean 3.3 μg CH_4 m^{-2} hr^{-1}, range -10.1 to 267), with 69% of measurements indicating methane emissions. This contrasted sharply with upland soils, which acted as strong methane sinks (mean

-90.9 µg CH_4 m^{-2} hr^{-1}, range -247.8 to -25.4), with 100% of measurements showing methane consumption. At intermediate sites, tree fluxes remained predominantly positive but lower in magnitude (mean 0.6 µg CH_4 m^{-2} hr^{-1}, range -1.2 to 14.7), with 62% of measurements showing emissions. Soils at these sites maintained strong methane consumption (mean -77.7 µg CH_4 m^{-2} hr^{-1}, range -263.4 to -13.4), comparable to upland sites despite higher soil moisture.

In transitional wetland sites, trees showed the highest emission rates (mean 7.5 µg CH_4 m^{-2} hr^{-1}, range -0.8 to 183.8), with 78% of measurements positive. Soils in these areas exhibited extreme variability, with a mean flux of 105.9 µg CH_4 m^{-2} hr^{-1} but ranging from -127.2 to 3,642.6 µg CH_4 m^{-2} hr^{-1}. The median soil flux in transitional wetlands was -6.0 µg CH_4 m^{-2} hr^{-1}, indicating that despite occasional high emission events, these soils frequently consumed methane (60% of measurements were negative).

These results highlight a clear distinction between tree-mediated methane emissions and soil methane fluxes across different landscape positions. While upland soils act as strong methane sinks, upland tree stems are consistent methane sources, with a one-sample t-test confirming that upland tree fluxes were significantly greater than zero ($p = 0.017$). This indicates that methane produced within tree tissues contributes to net ecosystem methane exchange even in methane-consuming soils. In contrast, transitional wetland sites show high variability in both tree and soil fluxes, with episodic conditions that can shift soils from sinks to sources, emphasizing the importance of landscape context and moisture dynamics in determining net methane fluxes.

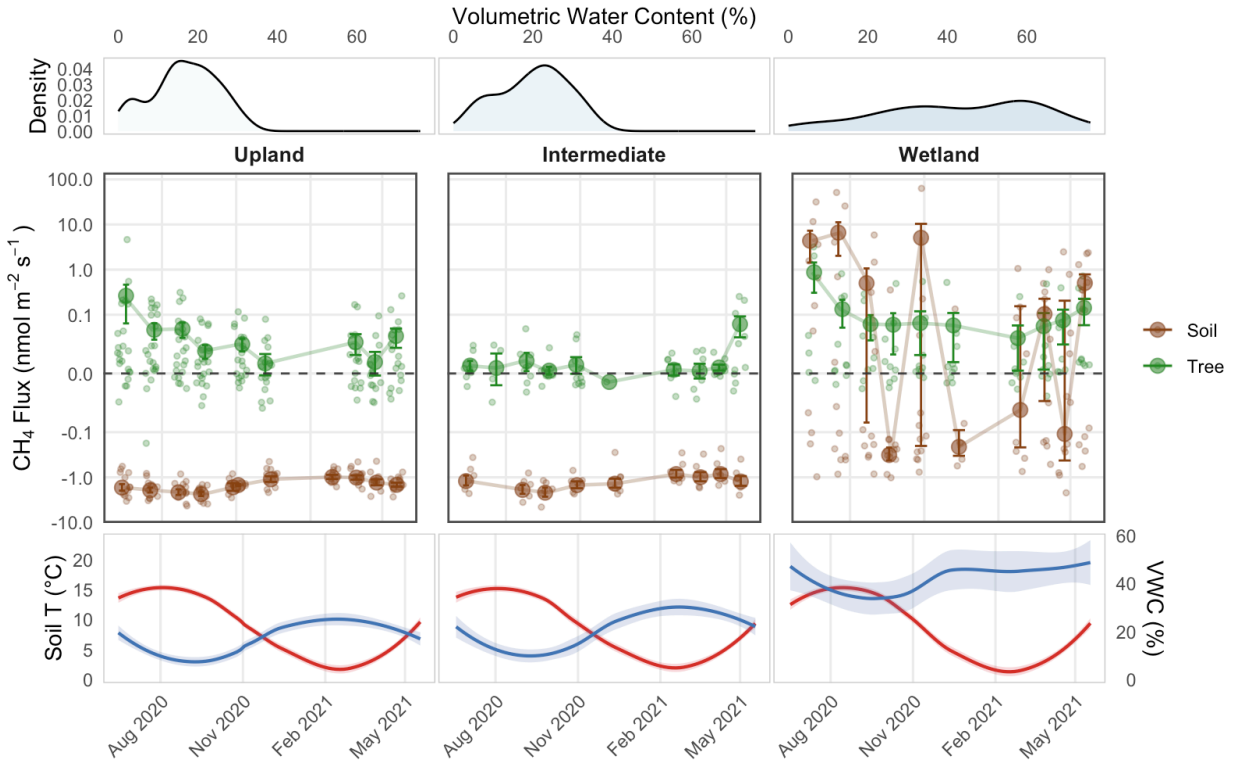

Figure 1. Temporal patterns of methane fluxes from tree stems and soils across a hydrological gradient at Yale-Myers Forest, Connecticut, June 2020 to May 2021. Data represent 342 tree flux measurements from 41 trees and 276 soil measurements from 12 soil plots, collected during 10 sampling campaigns. ***Top panel***: Distribution of volumetric water content (%) at 12 cm depth across upland (mean 16.7 ± 8.2%, n=121), intermediate (mean 20.0 ± 8.7%, n=47), and transitional wetland (mean 42.8 ± 19.4%, n=119) sites, showing three distinct hydrological zones. ***Middle panel***: CH_4 flux measurements from tree stems (green) and soils (brown) with individual measurements shown as semi-transparent points and mean values ± SE for 7-day intervals as solid points connected by lines. Data displayed on pseudo-logarithmic scale with dashed line at zero flux. Upland sites showed tree emissions averaging 0.057 nmol m^{-2} s^{-1} contrasting with soil consumption of -1.57 nmol m^{-2} s^{-1}. Intermediate sites showed tree emissions of 0.011 nmol m^{-2} s^{-1} and soil consumption of -1.35 nmol m^{-2} s^{-1}. Transitional wetland trees averaged 0.129 nmol m^{-2} s^{-1} emissions while soils showed high variability (mean 1.83, median -0.104 nmol m^{-2} s^{-1}). ***Bottom panel***: Seasonal dynamics of soil temperature (red, ranging -0.7 to 19.3°C) and volumetric water content (blue) as loess-smoothed curves.

2. Methane Flux by Height and Analysis of Height Effects

Methane flux measurements at three stem heights (0.5, 1.25, 2.0 m) showed consistent positive fluxes for most upland species. Linear mixed-effects models revealed significant height effects in only 3 of 11 species tested. *Betula alleghaniensis* showed the strongest negative relationship (-0.824 nmol m^{-2} s^{-1} per meter stem height, $p = 0.002$), with fluxes decreasing from 1.52 ± 0.52 nmol m^{-2} s^{-1} at 0.5 m to 0.29 ± 0.08 nmol m^{-2} s^{-1} at 2.0 m. This robust effect (100% jackknife iterations significant; 11/14 trees with negative slopes) occurred where soil moisture (35.9% VWC) and soil methanogens ($10^{4.8}$ mcrA copies g^{-1}) were highest.

Tsuga canadensis (eastern hemlock) also showed a robust but much weaker negative height effect (-0.019 nmol m^{-2} s^{-1} per meter, $p = 0.025$; approximately 2% the magnitude of *B. alleghaniensis* effect), with 82% of jackknife iterations remaining significant and 71% of individual trees showing negative slopes. In contrast, *Acer saccharum* (sugar maple) displayed a positive relationship (+0.200 nmol m^{-2} s^{-1} per meter, $p = 0.050$) that was not robust, with only 44% of jackknife iterations remaining significant, driven largely by an exceptionally high flux value (1.94 nmol m^{-2} s^{-1}) observed at 2 m on one tree. When this outlier was removed, the height effect became weaker but remained positive (+0.056 nmol m^{-2} s^{-1} per meter, $p = 0.022$).

Across all species, height effect coefficients showed a strong negative correlation with soil methanogen abundance ($r = -0.76$, $p = 0.007$), indicating that species in areas with higher soil methanogens were more likely to show decreasing flux with height—a pattern consistent with soil-to-stem transport. The correlation with soil moisture alone was weaker and non-significant ($r = -0.41$, $p = 0.21$), though soil moisture and methanogen abundance were positively correlated ($r = 0.50$, $p < 0.001$).

The absence of height-dependent flux patterns in 8/11 species, combined with the strong correlation between estimated height effect and soil methanogen abundance, supports a dual-mechanism model: trees in high soil methanogen environments show height-dependent patterns

typically considered indicative of soil-to-stem transport, while trees in typical upland conditions with low soil methanogens exhibit lower but uniform vertical profiles, at least to 2m height, potentially consistent with internal production.

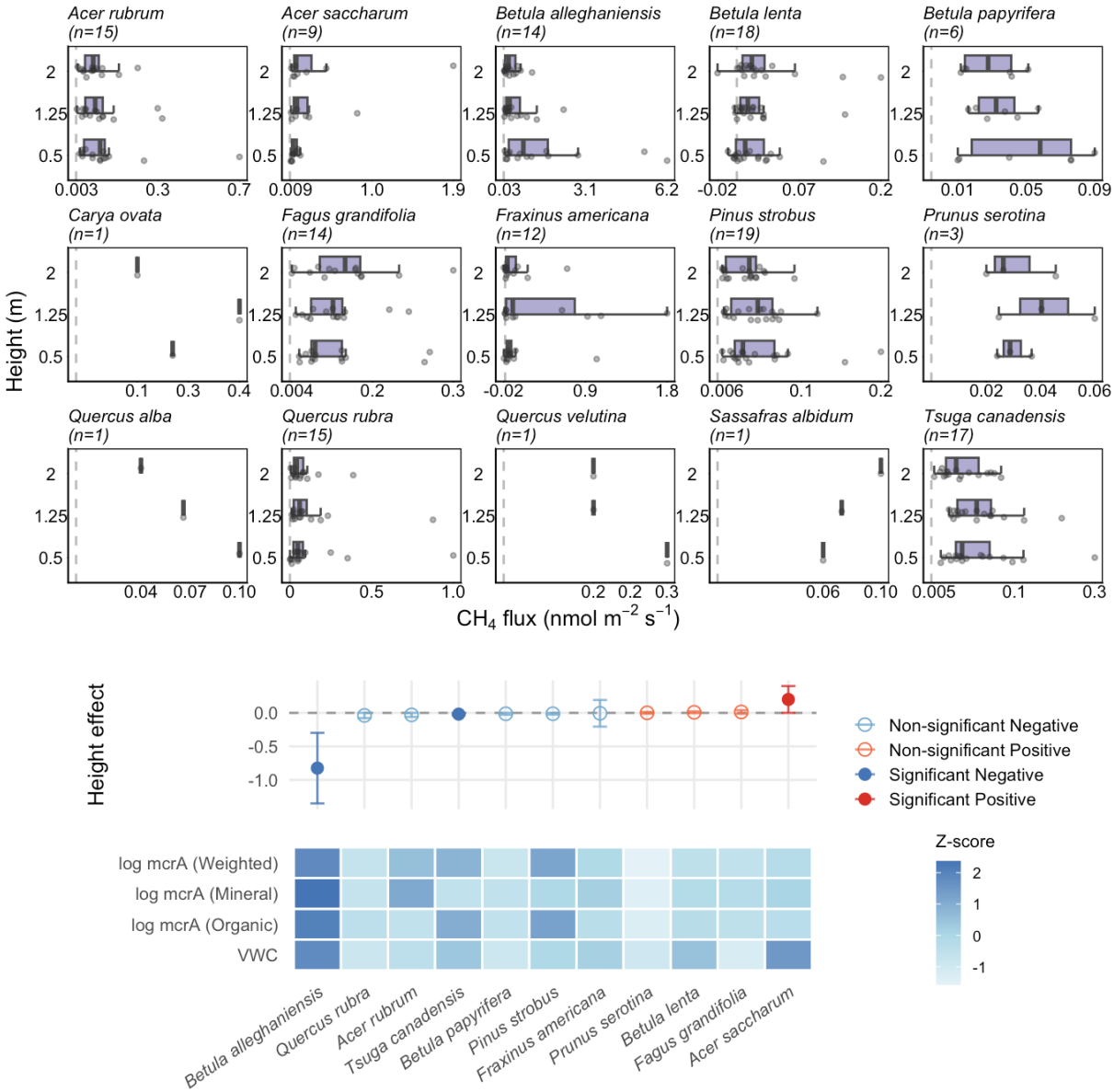

Figure 2. Methane flux patterns across stem heights and relationships with environmental drivers in upland forest tree species at Yale-Myers Forest, Summer 2021. Data from 434 flux measurements across 146 individual trees. Trees with multiple height measurements enabled mixed-effects modeling to separate within-tree from between-tree variation. **Top panel:** CH_4 flux measurements at three heights (0.5, 1.25, 2.0 m) for 15 tree species. Half-violin boxplots show flux distributions with individual measurements as jittered points (gray). Boxes indicate interquartile range with median; dashed horizontal lines indicate zero flux. Species arranged by height effect coefficient from most negative (left) to most positive (right). Sample sizes indicate number of individual trees per species. **Middle panel:** Height effect coefficients (nmol m^{-2} s^{-1} per cm) from linear mixed-effects models with 95% confidence intervals. Points and error bars colored by significance and direction: significant negative effects shown

in blue (Betula alleghaniensis $p = 0.002$, Tsuga canadensis $p = 0.025$), significant positive in red (Acer saccharum $p = 0.050$), non-significant negative in light blue, and non-significant positive in light red. Solid circles indicate $p < 0.05$; open circles indicate $p \geq 0.05$. **Bottom panel:** Environmental correlates as z-score normalized heatmap. Variables include volumetric water content (VWC) and $\log_{10}$-transformed soil methanogen abundance (mcrA gene copies g^{-1}) in organic, mineral, and depth-weighted soil layers. Blue intensity indicates relative values with darker blue representing higher z-scores. Species ordered to match middle panel. Height effect coefficients showed strong negative correlation with soil methanogen abundance ($r = -0.76$, $p = 0.007$).

3. Species Trends in Flux and Individual Variance Partitioning

Pooling breast-height (1.25 m) flux measurements from peak growing season surveys in 2021 and 2023 (n = 476 measurements; 141 from 2021, 335 from 2023) revealed substantial variation both within and among species. These measurements were primarily from upland forest sites where soils typically consume atmospheric methane. To quantify the relative importance of different factors driving flux variation, we conducted variance partitioning analysis using linear models that sequentially included environmental variables (temperature, moisture, tree diameter), species identity, and their interactions. This analysis revealed that species identity explained only 5.3% of variance, species-environment interactions 8.7%, environmental factors alone <0.01%, leaving 82.9% unexplained at the individual tree level.

Betula alleghaniensis (yellow birch) showed the highest mean emissions (0.279 ± 0.091 nmol m^{-2} s^{-1}), followed by *Acer saccharum* (sugar maple, 0.188 ± 0.061 nmol m^{-2} s^{-1}) and *Acer rubrum* (red maple, 0.170 ± 0.060 nmol m^{-2} s^{-1}). Gymnosperms including *Tsuga canadensis* (eastern hemlock, 0.026 ± 0.007 nmol m^{-2} s^{-1}) and *Pinus strobus* (white pine, 0.021 ± 0.010 nmol m^{-2} s^{-1}) exhibited consistently lower emissions.

The dominance of unexplained individual variance (82.9%) indicates tree-specific characteristics—potentially heartwood development, internal decay, microbial colonization history, wounding, bark features, gas flowpaths, or physiological status—drive emissions more than species identity or environmental conditions. Species-environment interactions (8.7%) suggest differential environmental responses among species, though these remain secondary to individual variability in upland forests.

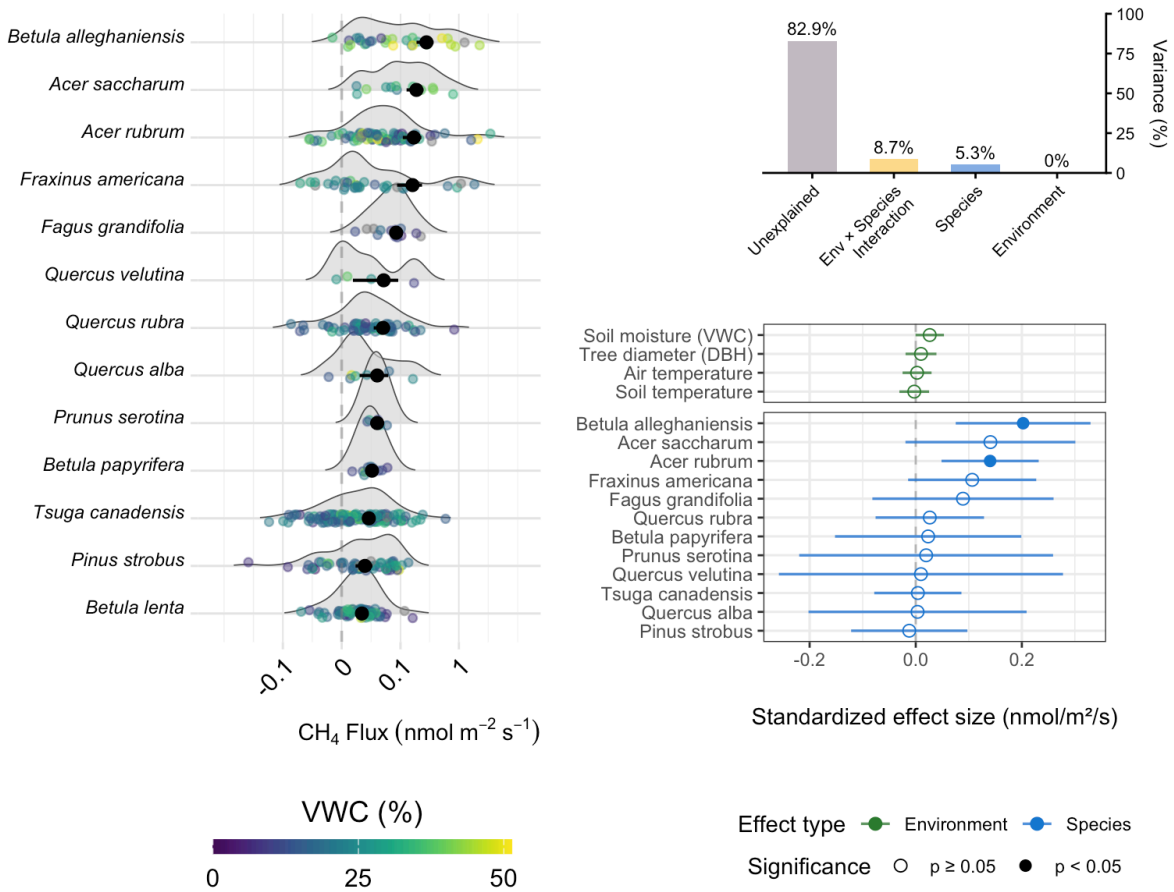

Figure 3. Variance partitioning and species-level patterns of methane flux from upland forest trees. Data from 476 breast-height (1.25 m) flux measurements across 13 species during peak growing season (summer) surveys in 2021 and 2023 at Yale-Myers Forest upland sites. **Left panel:** Ridge density plots showing distribution of CH_4 flux by species, with individual measurements colored by soil volumetric water content (VWC). Black points with error bars show mean ± SE. Species ordered by mean flux. **Top right panel:** Variance components from linear models showing the proportion of flux variance explained by unexplained individual variation (82.9%), species-environment interactions (8.7%), species identity (5.3%), and environmental factors (<0.01%). **Bottom right panel:** Standardized effect sizes from full model showing environmental (green) and species (blue) effects with 95% confidence intervals. Solid points indicate $p < 0.05$; open points indicate $p \geq 0.05$.

4. Quantifying Methanogens and Methanotrophs Across Tree and Soil Compartments

In a survey of 155 standing trees encompassing 16 species sampled during summer 2021, the vast majority harbored detectable methanogenic archaea within their living wood. Heartwood was particularly enriched in methanogens, with 97% of samples containing detectable mcrA genes. Among positive samples, mean abundance was $10^{3.2}$ copies g^{-1} dry wood (median $10^{2.7}$), with maximum values reaching $10^{6.9}$ copies g^{-1} in *Acer saccharum* (sugar maple). Over half (54%) of heartwood samples exceeded 500 mcrA copies g^{-1}. Sapwood showed significantly lower methanogen abundance (Wilcoxon rank-sum test, $p < 0.001$), with 69% of samples detectable, averaging $10^{2.3}$ copies g^{-1} (median $10^{2.1}$, max $10^{4.2}$) among positive samples.

Methanogens were substantially less abundant in soils surrounding trees. Only 59% of mineral soil samples and 53% of organic soil samples contained detectable methanogens. Among positive samples, mineral soils averaged $10^{1.9}$ copies g^{-1} wet soil (median $10^{1.6}$, max $10^{5.5}$), while organic horizons averaged $10^{2.0}$ copies g^{-1} (median $10^{1.6}$, max $10^{5.6}$). Given average soil moisture of 21% VWC, the median difference between heartwood and soil methanogen abundances exceeded one order of magnitude, with only 6-8% of soil samples exceeding 500 mcrA copies g^{-1}. Notable exceptions occurred in transitional wetland positions, particularly around *Betula alleghaniensis*, where soil methanogens reached $10^{5.5–5.6}$ copies g^{-1}.

Methanotrophs showed inverse abundance patterns. Combined pmoA and mmoX abundances were lowest in heartwood ($10^{3.3}$ copies g^{-1}), intermediate in sapwood ($10^{3.5}$ copies g^{-1}), and highest in soils ($10^{4.9}$ copies g^{-1} in both horizons). This inverse relationship suggests spatial segregation of methane production and consumption processes.

Based on controlled spiking experiments with wood samples that we performed in related work (Arnold et al 2024), wood DNA extraction recovers approximately 20% of target sequences, with losses occurring during freeze-drying, cryo-grinding, and extraction steps. Thus, actual wood methanogen abundances could potentially exceed our measurements by approximately 5-fold.

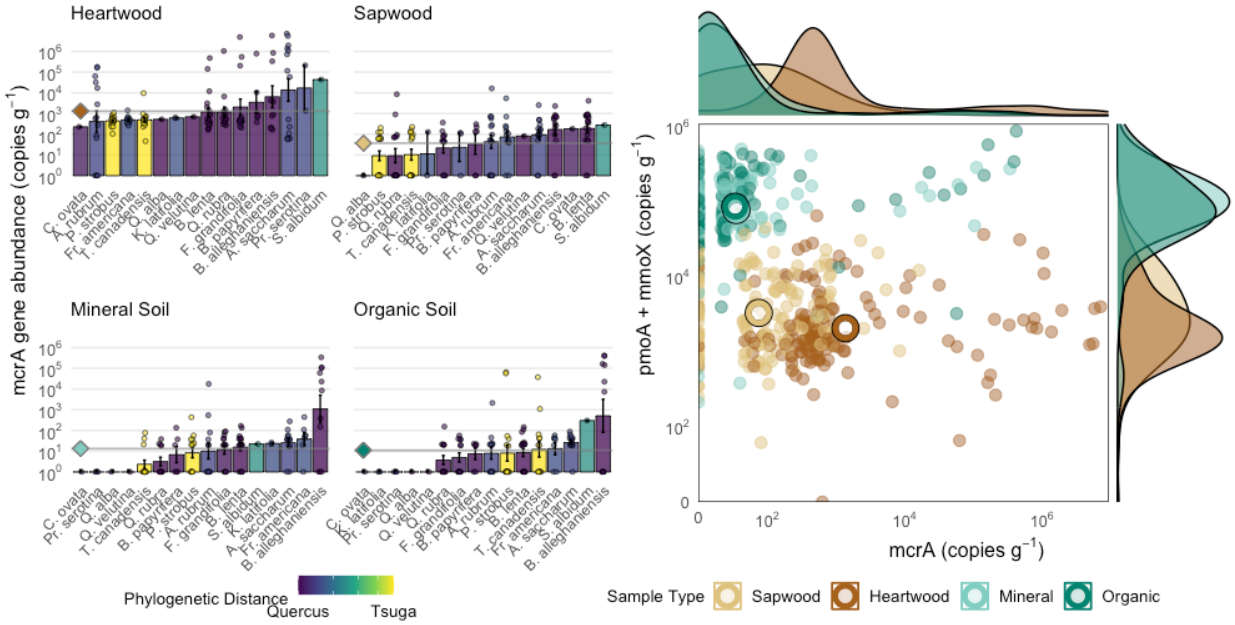

Figure 4. Methanogen and methanotroph abundance across forest compartments from summer 2021 survey. Left panel: Methanogen abundance (mcrA gene copies g^{-1}) across 16 tree species and four forest compartments at Yale-Myers Forest, measured by droplet digital PCR with probe-based assays. Bars show mean ± SE on $\log_{10}$ scale. Species ordered by mean abundance within each compartment; bar colors represent phylogenetic distance. Horizontal lines indicate compartment-wide geometric means. Sample sizes shown for each species. **Right panel:** Relationship between methanogen (mcrA) and methanotroph (pmoA + mmoX) abundance across forest compartments on pseudo-log scales. Points represent individual samples colored by compartment type. Marginal

density plots show distributions for each axis. Centroids (circles with black borders) indicate geometric mean values for each compartment. n = 147 heartwood, 154 sapwood, 128 mineral soil, 135 organic soil samples.

5. Community and Taxonomic Identity of Methanogens

16S rRNA sequencing corroborated the ddPCR findings, revealing that methanogens constitute a significant portion of the wood microbiome. In heartwood, methanogens ranged from 0 to 56.4% of all microbial taxa (mean 3.3±9.3%), while in sapwood they ranged from 0 to 6.37% (mean 0.096±0.61%). Methanogen abundance varied significantly by tree species (ANOVA: 16S rRNA $p<0.01$, ddPCR $p<0.05$), with certain trees serving as preferential hosts. *Acer saccharum* heartwood contained the highest methanogen concentrations both in absolute terms ($10^{5.13}\pm10^{2.11}$ copies g^{-1}, $p<0.1$) and as a proportion of the total microbiome (15.7±13.0%, $p<0.001$). In contrast, conifer species including *Pinus strobus* and *Tsuga canadensis* harbored the lowest methanogenic loads ($p<0.01$), averaging approximately $10^{3.6}$ copies g^{-1} in heartwood and $10^{1.4}$ copies g^{-1} in sapwood.

The wood methanogenic community was dominated by two taxonomic families. Methanobacteriaceae comprised 2.65±8.12% of heartwood communities on average but reached up to 56.3% in some samples, while in sapwood they ranged from 0-6.37%. Methanomassiliicoccaceae showed lower but still substantial abundances, averaging 0.63±2.42% in heartwood with a maximum of 17.1%, and 0-0.63% in sapwood. Both families were significantly more abundant in heartwood than sapwood ($p<0.001$). Other methanogenic groups occurred only at trace amounts, with the third most abundant family, Methanosarcinaceae, peaking at just 1.29% of the total community.

Soil methanogenic communities differed markedly from those in wood, being dominated by Bathyarchaeia rather than wood-associated families. While trace amounts of Methanobacteriaceae were detected in soils (mineral: 0.025±0.16%, organic: 0.032±0.19%), Methanomassiliicoccaceae was virtually absent from soil samples. Meanwhile, methanotrophs (known and potential/facultative) were elevated in soils, with different taxonomic composition compared to wood (Fig. S1-S2). This compositional divergence between wood and soil communities argues against passive colonization from soil and suggests selection for specific methanogenic lineages adapted to the wood environment.

These two dominant wood-associated families utilize distinct metabolic pathways. Methanobacteriaceae are hydrogenotrophic, primarily reducing CO_2 using H_2 or formate as electron donors. Methanomassiliicoccaceae are methylotrophic, performing hydrogen-mediated reduction of methyl groups from compounds such as methanol and potentially lignin-derived substrates. The co-occurrence of these metabolically distinct groups indicates that multiple pathways support methanogenesis within living wood, reflecting the diverse chemical environments and substrate availability within tree tissues.

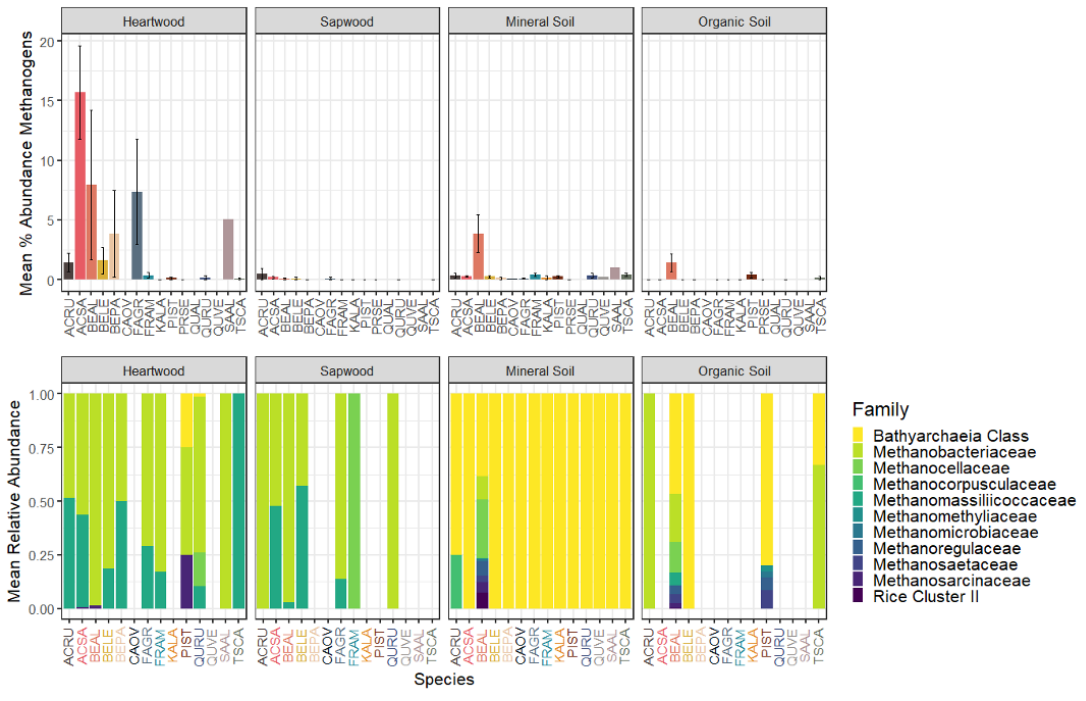

In

Figure 5: Methanogenic taxa relative abundance in tree and soil samples. (a) Methanogen relative abundance (percentage of total prokaryotic community) based on 16S rRNA gene sequencing across tree species and forest compartments. Data shown for heartwood, sapwood, mineral soil, and organic soil for 16 tree species at Yale-Myers Forest. (b) Methanogen taxonomic composition showing relative abundances of major methanogenic families across tree species and forest compartments. Stacked bars represent proportion of different methanogenic taxa.

6. Taxonomic Correlations and Inferred Metabolic Pathways

FAPROTAX analysis of 16S rRNA data (Fig. S2) suggested potential metabolic capabilities of detected taxa. Fermentation-related metabolisms were predicted to comprise 16.6% of heartwood and 6.8% of sapwood communities. Putative dark hydrogen oxidation, which requires H_2 availability, appeared enriched in heartwood (3.69%) compared to sapwood (1.15%, $p<0.1$), with the highest values (11.8%) in *Acer saccharum*. Predicted methylotrophy was also more frequent in heartwood (0.64%) than sapwood (0.02%, $p<0.001$), peaking at 5.07% in *Acer saccharum* heartwood ($p<0.001$). These inferred functions are consistent with the availability of hydrogen and methyl substrates that could support methanogenesis, although competition between methylotrophs and methanogens is also possible.

PICRUSt2 functional inference (Fig. S3) indicated differences in predicted metabolic pathways between heartwood and sapwood segments. Heartwood showed greater representation of methanogenesis-associated pathways, including reductive acetyl-CoA, H_2/CO_2 methanogenesis, and acetate methanogenesis. These co-occurred with predicted fermentation pathways (homolactic fermentation, mannan degradation, L-arginine biosynthesis) that may provide hydrogen, acetate, and formate substrates for methanogens. Sapwood, by contrast, was enriched

in predicted aerobic pathways such as purine nucleotide degradation and heme biosynthesis, along with cell wall synthesis pathways including peptidoglycan and teichoic acid biosynthesis.

Significant correlations with *mcrA* gene copy number, quantified by ddPCR, revealed that Christensenellaceae and Lachnospiraceae were consistently associated with methanogens (Methanobacteriaceae and Methanomassiliicoccaceae). These associations are consistent with known syntrophic relationships, in which fermentative bacteria generate metabolites that are consumed by methanogens. Christensenellaceae are obligate anaerobes that ferment polysaccharides and proteins, yielding short-chain fatty acids and hydrogen (Morotomi et al. 2012); Lachnospiraceae are versatile fermenters of plant-derived carbohydrates that produce acetate, butyrate, lactate, formate, and hydrogen (Kaminsky et al. 2023; Zaplana et al. 2024) Together, these families provide substrates that could sustain methanogenic archaea. Methanobacteriaceae are hydrogenotrophic methanogens that reduce CO_2 with H_2 to methane, while Methanomassiliicoccaceae are methylotrophic methanogens that use methanol and methylamines with H_2 as an electron donor (Buan 2018; Boone et al. 2015; Cozannet et al. 2020). Their significant association with *mcrA* copy number therefore supports the interpretation of potential complementary metabolic roles that facilitate methane production in anoxic microenvironments.

The spatial distribution of these pathways corroborate a redox gradient within tree tissues. Inner core segments appear to be more reduced and favor anaerobic processes, such as fermentation and methanogenesis, while outer core segments are more oxidized, favoring aerobic metabolism. These findings align with redox stratification, where metabolic processes occur along a gradient from oxygen-rich to oxygen-depleted zones within tree stems, and align with our recent results from related work finding higher methane and more variable oxygen in heartwood compared to sapwood in trees at this site (Arnold and Gewirtzman et al. 2025).

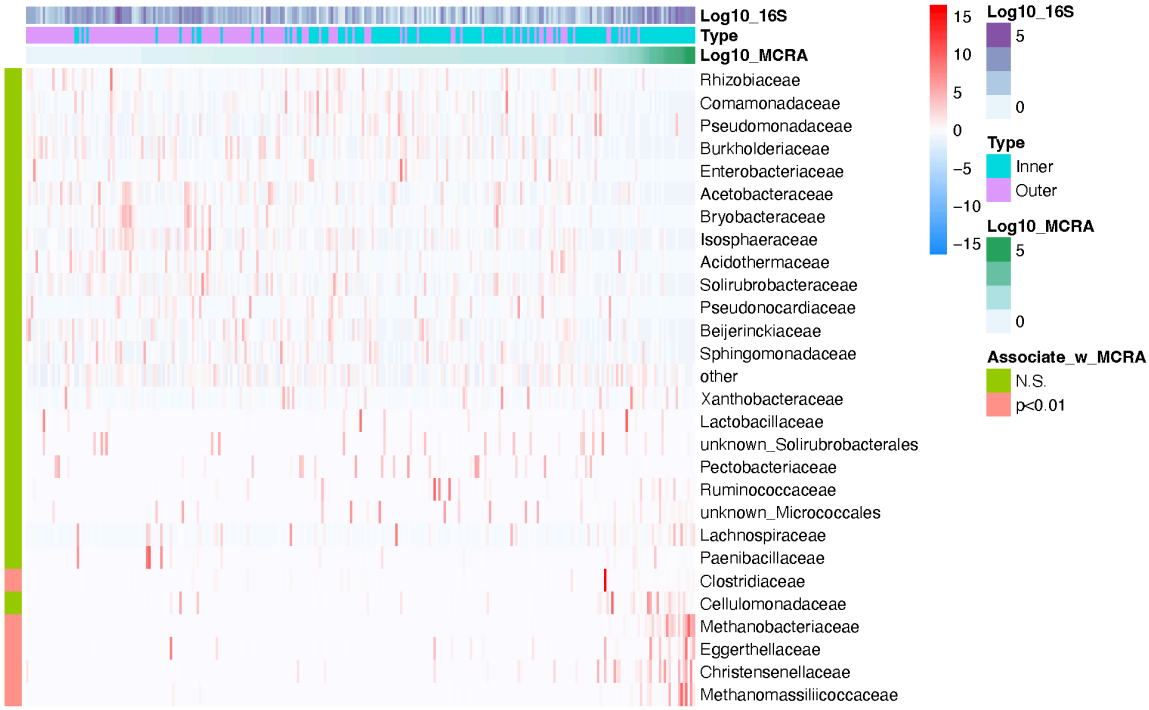

Figure 6: Heatmap showing microbial community composition and methanogen abundance across tree core samples from Yale-Myers Forest. The figure displays bacterial family abundance (log10 16S rRNA gene copies) with samples organized by core type (inner vs. outer) and methanogen abundance (log10 mcrA gene copies). Each column represents an individual tree core sample, with the top color bars indicating 16S rRNA abundance, core type (teal for inner, purple for outer), and mcrA abundance (green gradient). Bacterial families are listed on the y-axis, with red intensity indicating relative abundance within each sample. Families significantly associated with methanogen abundance ($p<0.01$) highlighted on the left margin; non-significant associations are shown in green. Key methanogenic families (Methanobacteriaceae, Christensenellaceae, Methanomassiliicoccaceae) appear at the bottom, showing higher abundance in samples with elevated mcrA levels, particularly in inner core samples.

7. Individual-Level Gene-Flux Relationships and Sampling Limitations

At the individual tree level, correlations between microbial gene abundances and methane flux were weak. Methanogen abundance (mcrA) showed $R^2 < 0.1$ for both heartwood and sapwood, while methanotroph genes (pmoA, mmoX) showed similarly weak relationships (see SI). The methanogen:methanotroph ratio also failed to predict individual tree flux ($R^2 < 0.01$) at the level of individual trees. These weak correlations likely reflect the heterogeneous distribution of microbial communities within tree tissues, given increment boring samples only a small fraction of stem volume. Correlations were similarly positive but weak between methanogen abundance and stem internal methane concentration (Fig. S4-S5).

The sampling limitations were dramatically illustrated in an intensively sampled black oak (*Quercus velutina*) with measurements at seven heights (0-10 m). Methane fluxes peaked at mid-stem heights (4-6 m) rather than showing uniform or exponentially decreasing patterns,

corresponding with the upper limit of visible heart rot. Internal methane concentrations exceeded 1,500 ppm at these heights, yet mcrA abundance from cores varied by over three orders of magnitude, with some samples showing no detectable methanogens despite elevated gas concentrations.

This mismatch between gas concentrations and microbial abundance indicates that methane production may occur in localized hotspots associated with decay pockets or anaerobic microsites rather than being uniformly distributed throughout the stem. These hotspots may drive emissions yet be easily missed by standard increment core sampling, which would not adequately capture the small-scale patchiness of methanogenic communities. The poor individual-level correlations reflect regression attenuation: when measurement error in the independent variable (mcrA abundance) is high due to inadequate spatial sampling, the observed correlation with the dependent variable (flux) becomes systematically weakened.

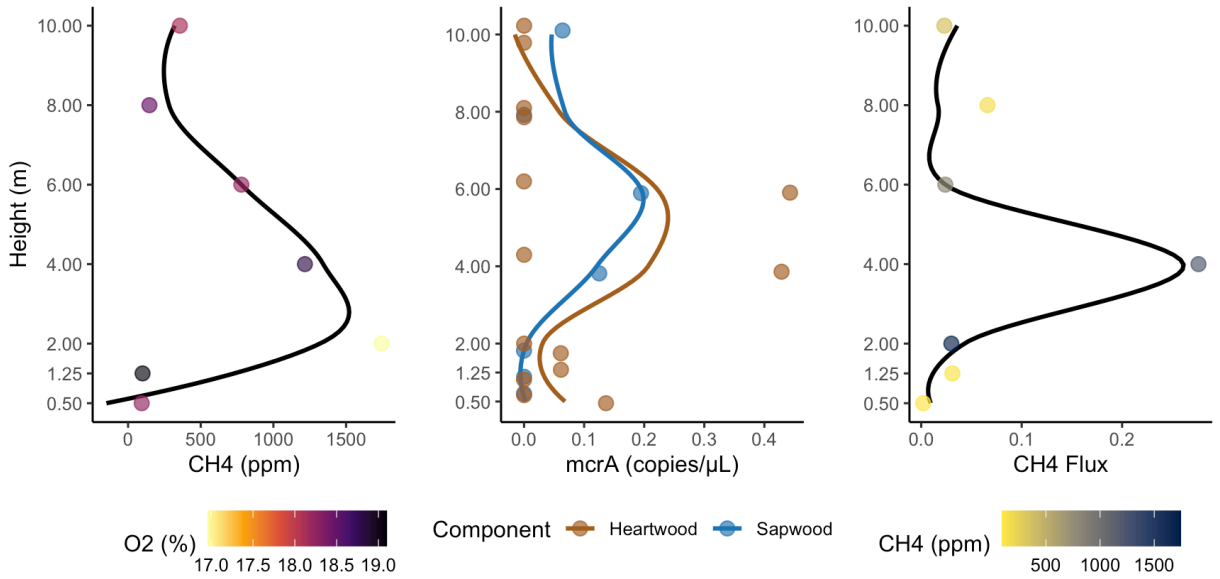

Figure 7: Vertical profiles of internal gas concentrations, methanogen abundance, and methane flux in a felled black oak (Quercus velutina) tree at Yale-Myers Forest. All measurements taken at seven heights along the stem (0-10 m): (Left) Internal methane concentrations (CH_4 ppm) with points colored by oxygen percentage (17.0-19.0%, yellow to purple gradient). (Center) Methanogen abundance (mcrA gene copies/µL) in heartwood (brown circles) and sapwood (blue circles) samples, with fitted trend lines. (Right) Methane flux measurements (CH_4 flux units) along the stem height with points colored by internal methane concentration (500-1500 ppm, yellow to gray gradient). The black curves represent smoothed trend lines for each measurement.

8. Tree Species-Level Gene-Flux Relationships

We next examined whether aggregating data to species level would reveal patterns obscured by within-tree heterogeneity. For this analysis, we calculated area-weighted methanogen and methanotroph abundances by integrating densities from inner (heartwood) and outer (sapwood) samples, weighted by their respective cross-sectional areas.

Species-level aggregation revealed significant correlations absent at the individual level. While individual trees showed no relationship between area-weighted mcrA and flux ($R^2 < 0.001$, n = 122 trees), species-level medians showed strong positive correlation ($R^2 = 0.40$, $p = 0.049$ for log-transformed data; n = 10 species with ≥5 observations each). Methanotroph genes (pmoA + mmoX) showed a weak negative correlation with flux ($R^2 = 0.07$, $p = 0.467$).

The ratio of area-weighted methanogens to methanotrophs emerged as the strongest predictor of species-level flux, explaining 53.8% of variance ($R^2 = 0.538$, Pearson r = 0.711 on log-transformed ratio, $p = 0.016$). This ratio outperformed either gene group alone in model comparisons (AIC = -44.82 vs. -42.26 for mcrA alone), indicating that the balance between methane production and consumption processes better predicts emissions than production potential alone.

This scale-dependent pattern, where microscale heterogeneity obscures relationships that emerge at broader scales, is not wholly unexpected given the small size of tree cores, the known hotspot-driven spatial variability of methane production, and the limited mobility within wood. The dramatic improvement demonstrates that species-level averaging reduces measurement noise from spatial heterogeneity, revealing an underlying biological relationship between methanogen abundance and methane flux that sampling limitations obscure at finer scales (detailed modeling results in SI).

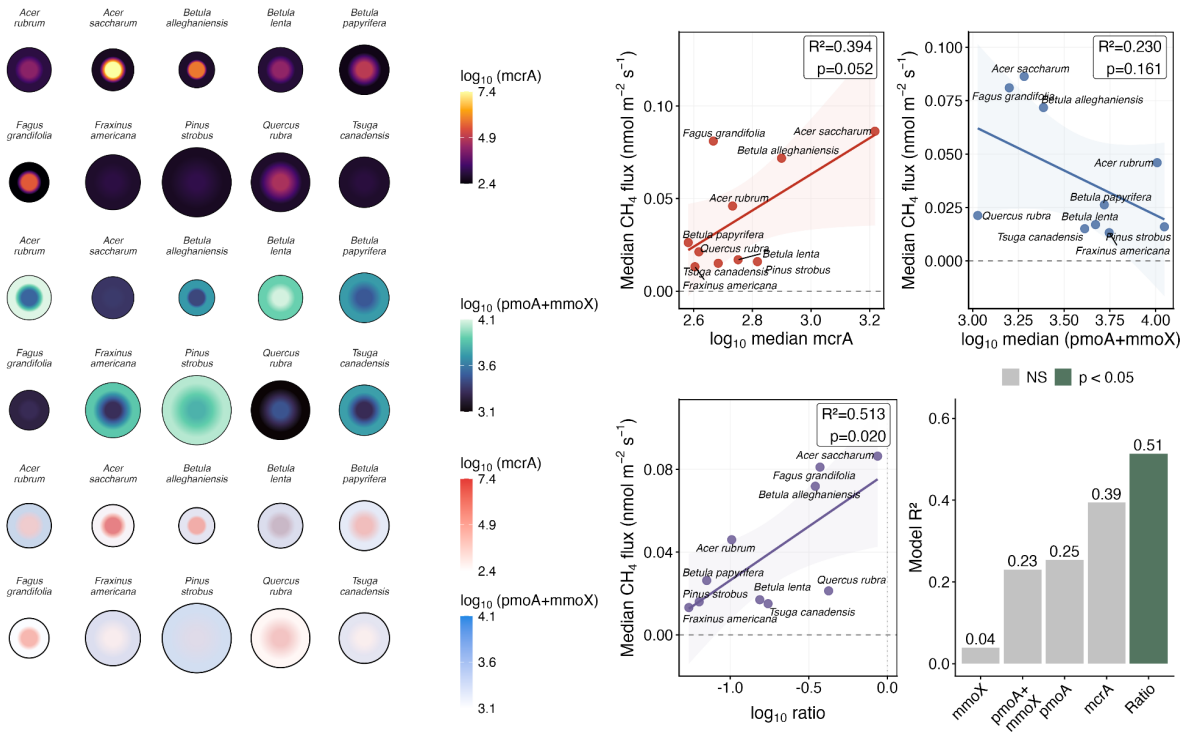

583

584 **Figure 8**: **Spatial distribution of methanogens and methanotrophs in tree stems and species-level gene-flux**
585 **relationships.** Left panels: Radial heatmaps for 10 species showing gene abundance patterns interpolated from
586 median heartwood (≤5 cm from pith) and sapwood (≤5 cm from bark) concentrations. Top: $\log_{10}$(mcrA) gene copies
587 g^{-1}. Middle: $\log_{10}$(pmoA+mmoX) gene copies g^{-1}. Bottom: Overlay of methanogen (red) and methanotroph (blue)
588 distributions. Circle diameter proportional to median species diameter at breast height. Right panels: Species-level
589 correlations (n = 10 species, ≥5 trees each) between median area-weighted gene abundance and median CH_4 flux.
590 Top left: mcrA. Top right: pmoA+mmoX. Bottom left: $\log_{10}$ ratio (mcrA/methanotrophs). Bottom right: R^2
591 comparison for linear regressions using mcrA, pmoA, mmoX, pmoA+mmoX, and ratio as predictors. All
592 regressions shown with 95% confidence intervals. Area-weighted values integrate heartwood and sapwood
593 concentrations weighted by cross-sectional area contributions.

594

595 **9. Random Forest Upscaling**

596 Random forest models trained on tree and soil flux measurements predicted seasonal flux
597 patterns across the forest plot (Fig. S6). The tree model achieved out-of-bag $R^2 = 0.15$, with
598 within-species standardized diameter, soil moisture, and species-specific moisture interactions
599 (particularly for *Betula alleghaniensis* and *Fraxinus americana*) as top predictors. The soil
600 model achieved $R^2 = 0.28$, with moisture-temperature interactions, soil moisture, soil
601 temperature, and seasonal cyclicity as dominant predictors. Models incorporated chamber type as
602 a predictor rather than applying post-hoc calibration. Feature importance was assessed using
603 impurity-based metrics.

On a per-unit-area basis, tree stem emissions averaged 0.07 nmol m^{-2} s^{-1} across the year (monthly means ranged from 0.04-0.12 nmol m^{-2} s^{-1}) while soil uptake averaged 1.76 nmol m^{-2} s^{-1} (monthly means: 1.58-2.05 nmol m^{-2} s^{-1}). Per unit area, stem emissions represented 4.2% of soil uptake, with peak emissions in July (0.12 nmol m^{-2} s^{-1}).

At our study site, based on lateral stem surface area of cylinders to 2 m height (3,555 m^2 across 10.2 ha, representing 3.47% of plot area), tree emissions contributed 0.003 nmol m^{-2} s^{-1} on a plot-area basis, totaling 1.3 mg CH_4 m^{-2} yr^{-1} and offsetting 0.14% of soil uptake (890 mg CH_4 m^{-2} yr^{-1}). As a scaling exercise, applying our per-unit-area stem flux to the woody area index of 3.07 reported for temperate forests (Gauci et al. 2024)—assuming constant emissions across all woody surfaces—would yield 114 mg CH_4 m^{-2} yr^{-1}, offsetting 13% of soil uptake. These estimates are based on measurements restricted to 0-2 m stem height and lack empirical data on vertical flux profiles or site-specific woody area above 2 m. While we observed no evidence of declining fluxes within our measurement range and detected a flux hotspot at ~4 m height in one tree measured to 10 m, insufficient data exist to constrain these uncertainties.

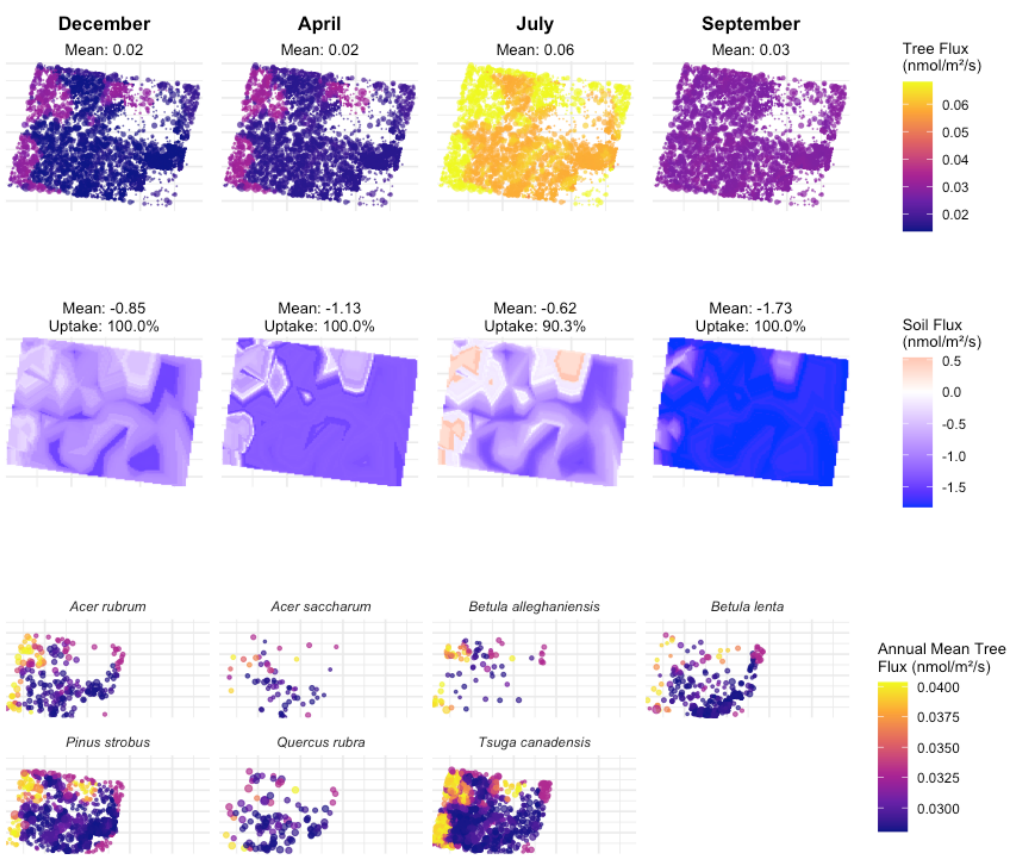

Figure 9: Integrated seasonal and species-level patterns of methane flux across tree and soil compartments at Yale-Myers Forest. Top panel: Monthly random forest-estimated tree stem methane flux for December, April,

July, and September, with individual trees represented as points colored by flux magnitude (nmol m^{-2} s^{-1}, plasma color scale) and sized proportionally to basal area (m^2). **Middle panel**: Corresponding estimated soil methane flux for the same months, displayed as interpolated raster surfaces. **Bottom panel**: Spatial distribution of annual mean tree CH_4 flux for common canopy species. Points colored by annual mean flux (nmol m^{-2} s^{-1}) and sized by basal area.

Discussion

Patterns of Tree Methane Emission from Upland to Wetland

Our study reveals that methane fluxes from trees vary significantly across landscape positions, with upland trees emitting lower levels of methane compared to trees in wetter, lowland areas. This gradient aligns with moisture availability and redox conditions of the surrounding environment. Upland soils are typically well-drained and oxygen-rich, conditions that promote methane oxidation by soil methanotrophs. Despite these soils consistently consuming atmospheric methane (mean -90.9 µg CH_4 m^{-2} hr^{-1}), trees in these areas still emit methane (mean 3.3 µg CH_4 m^{-2} hr^{-1}), suggesting internal methane production within tree tissues (Fig. 1).

Trees in transitional wetland areas exhibited the highest emission rates (mean 7.5 µg CH_4 m^{-2} hr^{-1}), where soils showed extreme variability—sometimes consuming, sometimes emitting methane. These higher tree emissions likely result from a combination of soil-derived methane transport (in areas with high soil methanogens like *Betula alleghaniensis* sites with $10^{4.8}$ mcrA copies g^{-1} soil), on top of equal or greater internal production by endophytic methanogens as compared to upland trees. The consistent methane emissions observed across tree species and landscape positions, even where soils are strong methane sinks, suggest internal production may be widespread among trees, though emission magnitude varies considerably between individuals.

Methane fluxes measured at multiple heights along tree stems showed no consistent pattern of decline with height across all but one of the upland tree species sampled, suggesting that the source of methane in upland trees may differ from the soil-originated methane typically observed in wetland trees (Fig. 2). In wetland environments, methane produced in anaerobic soils is commonly transported through tree stems via the xylem or internal gas spaces, resulting in higher fluxes near the base of the stem and an exponential decrease in methane flux with increasing height, as methane diffuses outward through stem tissues and into the atmosphere (Jeffrey et al. 2024; Anttila et al. 2024). This soil-origin transport pattern was not observed in the primarily upland tree species in this study.

Instead, methane fluxes in upland trees were relatively consistent across stem heights, indicating that methane production within the tree tissues themselves may be a more important contributor to methane flux in these environments. This pattern suggests that internal anaerobic niches within the tree stems—such as in the heartwood or other oxygen-depleted tissues—could serve as sites for methanogenic activity. The presence of methanogenic archaea in tree cores, as revealed through microbial community analysis, supports this hypothesis. These microbes are capable of producing methane in anaerobic microenvironments within tree tissues, independent

of soil methane transport (and were confirmed to do so in anaerobic incubations in related work; (Arnold et al. 2025).

Nonetheless, it is not possible to rule out some contribution from a soil origin. The observation of methane emissions from trees growing on methane-consuming soils does not necessarily indicate exclusive internal production. Multiple non-exclusive mechanisms could contribute to this apparent paradox (Pitz et al. 2018). Deep soil layers below the zone of active methanotrophy may harbor methanogenic communities whose products bypass surface oxidation through root uptake and xylem transport (Bhullar et al. 2013; Watson et al. 1997; Nouchi et al. 1990; Schimel 1995; Bradford et al. 2001). Anoxic microsites within otherwise aerobic soils, associated with aggregate interiors, root detrituspheres, or temporarily saturated zones, could serve as methane sources (Lacroix et al. 2023; Zausig et al. 1993; Keiluweit et al. 2018). While our soil sampling indicated a minimal role of soil methanogens in these communities, further work with RNA and isotopic tracers could provide further confirmation to link with rates. Further, it is important to note that the lack of decrease of flux within the lower portion of the stem could break down with measurements to higher heights, where a trend could become apparent; or, likelier (as seen in our high-resolution sampling of a black oak; Fig. 7)), that unpredictable patterns may occur, with hotspots at different heights aboveground.

Prevalence of Methanogens in Living Trees

Among all trees sampled, virtually all harbored methanogenic communities. Among samples analyzed, 97.3% of surveyed trees harbored measurable methanogen populations in their heartwood, compared to 68.8% in sapwood, 58.6% in mineral soil, and 52.6% in organic soil (Fig. 4). With abundances reaching ~10^7copies g^{-1} in some samples, these are not incidental colonizers but established communities representing more than half of the total heartwood microbiome in extreme cases. The consistency of this pattern across multiple diverse species suggests that methanogen colonization of heartwood is a widespread phenomenon in temperate forests.

The two-order-of-magnitude enrichment of methanogens in wood relative to surrounding soils indicates that trees provide a unique and favorable habitat for these obligate anaerobes. Heartwood's low oxygen availability, resulting from limited gas diffusion and consumption by aerobic microbes, creates anaerobic microsites suitable for methanogenesis; and such patterns support an emerging understanding of a divergent prokaryotic heartwood microbiome in life and in death (Cregger et al. 2018; Arnold and Gewirtzman et al. 2025; Moll et al. 2018). The presence of fermentative bacteria capable of producing hydrogen and simple organic acids imply a source of electron donors, while wood polymers including lignin may supply methylated substrates for methylotrophic methanogens. While we can only infer function in this work, some co-occurring clades detected here (*Lachnospiraceae*, *Methanobacteriaceae*; Fig. 5) have been shown to demonstrate such syntrophic methane production through mechanisms such as interspecies hydrogen transfer in other environments (Ruaud et al. 2020).

The consistent presence of methanogens across diverse tree species (Yip et al. 2019; Harada et al. 2024; Feng et al. 2022; Zeikus & Henning 1975) raises intriguing questions about the evolutionary history and ecological significance of these associations. Tree-methanogen relationships may represent an ancient symbiosis predating the divergence of major tree lineages, or convergent colonization of a widespread ecological niche. The species-specific differences in methanogen abundance, with highest levels in *Acer saccharum* and lowest in conifers, could reflect variation in wood chemistry, heartwood formation processes, or historical association with methanogens. Further, the patterns suggest that long-term changes in tree species composition, forest management practices, or climate-driven shifts in wood properties such as moisture or substrate availability could substantially alter ecosystem-level fluxes resulting from these tree-hosted communities.

Distinct Methanogenic Communities in Wood vs Soil

The taxonomic composition of wood methanogens differs markedly from soil communities, with wood dominated by Methanobacteriaceae and Methanomassiliicoccaceae while soils harbor primarily Bathyarchaeia (Evans et al. 2015). This compositional divergence argues against passive colonization from soil and instead suggests selection for specific methanogenic lineages adapted to the wood environment. The co-occurrence of hydrogenotrophic (Methanobacteriaceae) and methylotrophic (Methanomassiliicoccaceae) methanogens indicates multiple metabolic pathways support methanogenesis within trees.

The syntrophic community structure revealed by co-occurrence analysis (Fig. 6) and functional predictions (Fig. S2-S3). provides mechanistic insight into how methanogenesis is sustained. The strong correlation between fermentation and methanogenesis pathways, combined with anticorrelation with aerobic processes, depicts a stratified microbial ecosystem where spatial segregation enables coexistence of incompatible metabolisms. This microscale heterogeneity within seemingly homogeneous wood tissue underscores the importance of considering trees as complex microbial habitats rather than sterile structural material.

Multi-scale Complexity in Linking Microbial Abundance to Methane Flux

The weak correlation between methanogen abundance and flux at the individual tree level reflects multiple layers of complexity in tree-mediated methane cycling that our current methods only partially capture. While we detected methanogens through DNA-based approaches targeting the mcrA gene, this provides only a census of potential methane producers. DNA abundance does not directly translate to metabolic activity (Rocca et al. 2015); dormant or inactive cells retain their genetic material, while actively transcribing populations may represent a small fraction of total community members. RNA-based approaches targeting mcrA transcripts, or proteomic and metabolomic analyses, would provide more direct measures of active

methanogenesis but present substantial technical challenges in wood tissues due to low biomass yields and complex matrix effects.

Beyond the limitations of molecular censusing, methane emissions represent the net result of multiple interacting processes operating across different spatial and temporal scales. Flux measurements integrate production, consumption, and transport processes that may be spatially and temporally decoupled. Production occurs in anaerobic microsites where methanogens are active; consumption happens wherever methanotrophs encounter methane under suitable conditions; and transport depends on wood anatomy, moisture content, and pressure gradients. Reactive transport further complicates this picture—methane may be oxidized during diffusion through aerobic zones, creating steep concentration gradients that influence both flux magnitude and spatial patterns.

The inclusion of methanotroph measurements helps untangle one layer of this complexity. While methanotrophs showed spatial distributions inverse to methanogens—concentrated in outer wood and soils rather than heartwood—their abundances at individual tree level also failed to predict flux. However, the methanogen:methanotroph ratio emerged as the strongest species-level predictor of flux ($R^2 = 0.54$), outperforming methanogen abundance alone ($R^2 = 0.40$) for species-level medians. This suggests that net emissions reflect the balance between production and consumption processes, but this balance only becomes predictive when averaged across the spatial heterogeneity within individual trees.

Yet, additional complexity remains. For example, tree physiology fundamentally shapes reactive transport processes through anatomical and physiological controls. Wood porosity determines gas diffusivity and the potential for advective transport. Species with ring-porous anatomy may facilitate rapid vertical gas movement through large earlywood vessels, while diffuse-porous species restrict transport to slower diffusive pathways. Sapflow dynamics create diurnal and seasonal pressure fluctuations that can enhance or suppress gas emissions (Barba, Poyatos, et al. 2019; Barba et al. 2021; Bréchet et al. 2025; Anttila et al. 2024). Radial cell architecture, including the presence of ray parenchyma, tyloses, and resin ducts, may create preferential flow paths that channel gases along specific routes rather than uniform radial diffusion (Sorz & Hietz 2006; Cŏté 1963). These anatomical features vary not only among species (with species-level variation implicitly captured in our models) but also within individual trees based on growth history, injury response, and position within the stem.

Furthermore, production, consumption, and transport processes operate on different timescales. Soil gas production and consumption can shift rapidly, on hourly to daily timescales (Parolari et al. 2021), while internal gas production within trees may build up more slowly, persisting for weeks to months in poorly ventilated or anaerobic stem tissues, and and transport rates may vary from minutes for advective flow (Jeffrey et al. 2024) to days for diffusive movement across centimeters of wood (Sorz & Hietz 2006).

Internal methane buildup further illustrates this temporal complexity. Elevated concentrations (approaching 10% in the highest samples; Fig. S4-S5) could result from either high production

rates in active methanogenic zones or low diffusivity creating accumulation even with modest production. The relationship between concentration and flux is non-linear and depends on boundary conditions, diffusion coefficients, and the connectivity of gas-filled pore spaces. Hot moments—periods of elevated flux—may occur when changes in atmospheric pressure, temperature, or tree water status suddenly enhance transport from zones of accumulated methane. Such episodic releases could contribute disproportionately to time-integrated emissions while being easily missed by discrete sampling (Bréchet et al. 2025; Anthony & Silver 2021).

Spatial heterogeneity presents perhaps the greatest challenge for linking microbial abundance to flux. Our intensive sampling of the black oak dramatically illustrated this issue: even within zones of elevated methane concentration and emission at 4-6 m height, increment cores showed only a 50% detection rate for methanogens (Fig. 7). This suggests extremely localized production sites—decay pockets, wound sites, or other anaerobic niches—that create methane plumes extending well beyond the source. Standard increment boring, which samples <0.1% of stem volume, has perhaps low probability of intersecting these hotspots. While we assume primarily radial diffusion drives emissions, methane originating from a small hotspot may diffuse three-dimensionally, creating an extended zone of elevated concentration and surface emission. The measured flux at any point on the bark surface thus integrates contributions from multiple potential sources at varying distances and depths within the stem.

Addressing these complexities requires methodological advances beyond our current approaches. High-resolution sampling combining multiple cores at various depths and heights could better capture the probability distribution of methanogenic zones. Physical reconstruction of wood anatomy through techniques like X-ray computed tomography would reveal the three-dimensional network of potential gas conduits and barriers. Combining such structural information with multi-point gas sampling and isotopic tracers could help distinguish soil-derived from internally-produced methane and map transport pathways (Megonigal et al. 2020). Time-series measurements capturing diurnal and seasonal dynamics would reveal the importance of hot moments and the relationship between environmental drivers and emission patterns.

From Individual Complexity to Species-Level Patterns

Despite this individual-level complexity (Fig. 3), the emergence of strong correlations when data are aggregated to species level and weighted by cross-sectional area suggests that species-average methanogen loads better reflect emission potential than point measurements (Fig. 8). This aligns with recent findings that tree microbiomes show species-level conservation (Arnold and Gewirtzman et al. 2025), indicating that wood chemistry, anatomy, and physiology create predictable niches for microbial colonization. Our observation that the methanogen:methanotroph ratio correlates most strongly with species-median flux ($R^2 = 0.54$), with methanogen abundance alone explaining $R^2 = 0.40$, demonstrates that species-characteristic traits influence both microbial communities and gas emissions, even amid substantial individual variation.

The dramatic improvement in correlation strength when aggregating from individual to species level parallels observations in soil systems where microscale heterogeneity obscures relationships that become apparent at larger scales (Nunan et al. 2020; Waring et al. 2016; Polussa et al. 2021). This reflects how averaging reduces noise from spatial heterogeneity and sampling error while preserving the underlying biological signal, illustrating the ecological principle that patterns obscured by fine-scale variation often emerge at broader scales of organization. For practical purposes, species-level relationships may prove more useful for predicting forest-scale methane budgets than attempts to characterize every individual tree's heterogeneous internal landscape.

Moving forward, reconciling individual and species-level patterns requires embracing this complexity rather than seeking simple universal relationships. Trees are not homogeneous chemical reactors but spatially structured habitats where microbial processes, physical transport, and plant physiology interact across multiple scales. Understanding these interactions demands interdisciplinary approaches combining microbial ecology, tree physiology, soil science, and transport physics—a synthesis that promises to reveal how living trees function as dynamic components of the global methane cycle.

Methodological Considerations

Our study highlights important methodological challenges in quantifying tree-associated methane cycling. The high spatial heterogeneity of methanogens within trees necessitates sampling strategies that capture representative volumes rather than point measurements. Future studies should consider computed tomography or other non-destructive imaging to map anaerobic zones within trees, combined with targeted sampling of these regions.

The dominance of unexplained variance at the individual tree level indicates that unmeasured factors strongly influence emissions. Potential drivers include tree health status, presence of heart rot or other decay, hydraulic properties affecting internal oxygen dynamics, and historical colonization events. Long-term monitoring of individual trees could help identify whether emissions are stable traits or vary with tree physiological status.

Implications for Forest Methane Budgets

Our results highlight a fundamental scaling challenge in quantifying tree contributions to forest methane budgets. At our site, based on lateral stem surface area to 2 m height (3.47% of plot area), tree emissions offset 0.14% of soil methane consumption (1.3 vs. 890 mg CH_4 m^{-2} yr^{-1}; Fig. 9). However, extrapolating our per-unit-area fluxes to a woody area index of 3.07 (Gauci et al., 2024), assuming constant emissions across all woody surfaces, yields 114 mg CH_4 m^{-2} yr^{-1} (13% offset). Whether tree emissions represent a negligible fraction or a substantial offset

depends critically on vertical flux patterns and total woody surface area, both of which remain largely uncharacterized.

Within our limited measurement range (0-2 m), we observed no evidence of declining fluxes with height, and detected a flux hotspot at ~4 m in the one tree measured to 10 m. Notably, we saw no evidence of a recently proposed switch to net uptake with increasing stem height (Gauci et al. 2024). However, these sparse observations cannot constrain vertical profiles across the canopy. Without systematic vertical profiling across multiple trees and species, we cannot determine whether our 0-2 m measurements accurately represent fluxes at canopy height.

Our upland site likely differs mechanistically from wetland systems in the source of tree-stem methane emissions. In wetlands, exponential decline in flux with height results from diffusive loss of soil-transported methane (Pangala et al. 2013; Barba, Bradford, et al. 2019). If upland tree emissions derive primarily from internal stem production rather than basal transport, emissions would scale with total woody surface area rather than proximity to soil. This mechanistic difference has critical implications for scaling: internal production suggests fluxes may remain substantial throughout the canopy, making measurements restricted to lower stems potentially unrepresentative of whole-tree contributions.

Resolving these uncertainties requires addressing two interconnected measurement challenges. First, quantifying woody surface area demands direct three-dimensional measurements rather than allometric estimates. Terrestrial laser scanning (TLS) offers promise for deriving site-specific woody area component measurements and allometries (Calders et al. 2020). Second, measuring stem fluxes throughout the canopy requires climbing, canopy access systems, towers, or walkways—infrastructure rarely available across sites or seasons. Top-down constraints from tower-based or airborne eddy covariance offer an alternative, allowing deduction of tree contributions from differences between net ecosystem and soil fluxes (Pangala et al. 2017). However, towers in upland forests remain sparse, and small tree emissions relative to dominant soil uptake may fall below detection limits or prove difficult to separate from contributions of nested wetland areas (Delwiche et al. 2021). The combination of low signal strength, high spatial variability, and limited infrastructure for canopy-scale measurements represents a major frontier in understanding tree-stem methane dynamics in upland forests.

Conclusions

This study demonstrates that upland temperate forest trees harbor abundant methane-cycling communities that drive consistent tree stem net methane emissions independent of soil processes. The discovery that wood provides a more favorable habitat for methanogens than surrounding soils, combined with evidence for specialized wood-adapted methanogenic communities, contributes to a shifting paradigm in our understanding of forest methane cycling. Tree emissions partially offset soil methane consumption, reducing the net sink strength of upland forests and

possibly representing a climate-relevant flux that may respond differently to environmental change than traditional soil-atmosphere exchange. However, gross methanotrophy on tree stems may in turn limit tree emissions, and determinants of its magnitude, and the balance of these gross processes, is an area demanding urgent investigation. Recognition of trees as active players in methane cycling invites revision of forest greenhouse gas budgets and consideration of how forest management practices influence this previously overlooked term in global budgets.

Acknowledgements

We thank Josep Barba, Claire Butler, Luke Jeffrey, Andrew Reinmann, Cade Brown, Ari Gewirtzman, Thomas Harris, Naomi Hegwood, Marsh Hlavka, Fiona Jevon, Ellie Jose, Jonas Karosas, Talia Kolodkin, Camila Ledezma, Laura Logozzo, Taylor Maavara, Naomi Norbraten, Alex Polussa, Adriana Rubenstein, Cyrena Thibodeau, Les Welker, Qespi Wood, Michelle Spicer, and Jackie Matthes for their contributions to this work. We acknowledge our additional collaborators on the forest inventory plot: Liza Comita, Mark Ashton, Simon Queenborough, Stuart Davies and Sean McMahon. We thank Yale School Forests, University of Minnesota Genomics Center, Yale Analytical and Stable Isotope Center, W.M. Keck Biotechnology Resource Laboratory, Yale Center for Genetic Analyses of Biodiversity, and Yale Chemistry Glass Shop for technical support and facilities access.

Funding

This research was supported by the National Science Foundation Graduate Research Fellowship, Yale-Myers Forest Kohlberg-Donohoe Fellowship, Yale Institute for Biospheric Studies Early Grant, Yale School of the Environment-Yale Institute for Biospheric Studies Fellowship, and Yale Planetary Solutions Project Seed Funding.

Competing Interests

The authors declare no competing interests.

Data Availability

The 16S rRNA amplicon sequencing data generated in this study have been deposited in the NCBI Sequence Read Archive (SRA) under BioProject accession number PRJNA1124946. Methane flux measurements, Methanogen and methanotroph abundance data (ddPCR), internal gas concentration data are available at Figshare: https://figshare.com/s/b781d3c5c24f1089ed5d?. Tree and soil characterization data, and associated metadata will be made available upon publication. R code for statistical analyses, Random Forest models, variance partitioning, and figure generation is available on GitHub: https://github.com/jgewirtzman/tree-methanogens and will be made public upon publication.

Author Contributions

J.G. and W.A. contributed equally to this work. J.G. and W.A. conceived and designed the research, curated and analyzed data, acquired funding, conducted fieldwork and laboratory investigations, developed methodology, administered the project, provided resources, developed software and code, supervised research activities, and validated results. M.T. contributed to conceptualization, curated data, conducted investigations, and developed methodology. C.M. performed formal analysis and developed software. J.G., W.A., and C.M. created visualizations. H.B. and D.W. curated data, conducted investigations, and developed methodology. N.W., K.K., and L.G. curated data and conducted investigations. C.R.B. and M.D. acquired funding, developed methodology, and provided resources. P.A.R. contributed to conceptualization, acquired funding, and supervised research. J.P. acquired funding, developed methodology, administered the project, provided resources, and supervised research. M.A.B. acquired funding, developed methodology, administered the project, and supervised research. J.G. wrote the original draft. All authors reviewed and edited the manuscript and approved the final version.

References

Anthony, T.L. & Silver, W.L., 2021. Hot moments drive extreme nitrous oxide and methane emissions from agricultural peatlands. *Global change biology*, 27(20), pp.5141–5153.

Anttila, J. et al., 2024. Model of methane transport in tree stems: Case study of sap flow and radial diffusion. *Plant, cell & environment*, 47(1), pp.140–155.

Arnold, W and Gewirtzman, J. et al., 2025. A diverse and distinct microbiome inside living trees. *Nature*, pp.1–10.

Arnold, W. et al., 2024. A method for sampling the living wood microbiome. *Methods in ecology and evolution / British Ecological Society*. Available at: https://besjournals.onlinelibrary.wiley.com/doi/10.1111/2041-210X.14311.

Barba, J., Bradford, M.A., et al., 2019. Methane emissions from tree stems: a new frontier in the global carbon cycle. *The New phytologist*, 222(1), pp.18–28.

Barba, J. et al., 2024. Methane emissions from tree stems - current knowledge and challenges: an introduction to a Virtual Issue. *The new phytologist*, 241(4), pp.1377–1380.

Barba, J. et al., 2021. Spatiotemporal variability and origin of CO2 and CH4 tree stem fluxes in an upland forest. *Global change biology*, 27(19), pp.4879–4893.

Barba, J., Poyatos, R. & Vargas, R., 2019. Automated measurements of greenhouse gases fluxes from tree stems and soils: magnitudes, patterns and drivers. *Scientific reports*, 9(1), p.4005.

Bates, D. et al., 2015. Fitting Linear Mixed-Effects Models Using \textbflme4. *Journal of statistical software*, 67(1). Available at: http://www.jstatsoft.org/v67/i01/ [Accessed September 16, 2021].

Bhullar, G.S., Edwards, P.J. & Olde Venterink, H., 2013. Variation in the plant-mediated methane transport and its importance for methane emission from intact wetland peat mesocosms. *Journal of plant ecology*, 6(4), pp.298–304.

Boone, D.R., Whitman, W.B. & Koga, Y., 2015. Methanobacteriaceae. *Bergey's Manual of Systematics of Archaea and Bacteria*, pp.1–1. Available at: http://dx.doi.org/10.1002/9781118960608.fbm00097.

Bradford, M.A. et al., 2001. Role of CH4 oxidation, production and transport in forest soil CH4 flux. *Soil biology & biochemistry*, 33(12-13), pp.1625–1631.

Bréchet, L.M. et al., 2025. Insights into the subdaily variations in methane, nitrous oxide and carbon dioxide fluxes from upland tropical tree stems. *The new phytologist*, 245(6), pp.2451–2466.

Buan, N.R., 2018. Methanogens: pushing the boundaries of biology. *Emerging topics in life sciences*, 2(4), pp.629–646.

Calders, K. et al., 2020. Terrestrial laser scanning in forest ecology: Expanding the horizon. *Remote sensing of environment*, 251, p.112102.

Callahan, B.J. et al., 2016. DADA2: High-resolution sample inference from Illumina amplicon data. *Nature methods*, 13(7), pp.581–583.

Carmichael, M.J. et al., 2024. Microbial Communities in Standing Dead Trees in Ghost Forests are Largely Aerobic, Saprophytic, and Methanotrophic. *Current microbiology*, 81(8), p.229.

Cŏté, W.A., Jr, 1963. Structural factors affecting the permeability of wood. *Journal of Polymer Science Part C Polymer Symposia*, 2(1), pp.231–242.

Covey, K.R. et al., 2012. Elevated methane concentrations in trees of an upland forest. *Geophysical research letters*, 39(15). Available at: https://agupubs.onlinelibrary.wiley.com/doi/abs/10.1029/2012GL052361 [Accessed March 10, 2021].

Covey, K.R. & Megonigal, J.P., 2019. Methane production and emissions in trees and forests. *The New phytologist*, 222(1), pp.35–51.

Cozannet, M. et al., 2020. New insights into the ecology and physiology of Methanomassiliicoccales from terrestrial and aquatic environments. *Microorganisms*, 9(1), p.30.

Cregger, M.A. et al., 2018. The Populus holobiont: dissecting the effects of plant niches and genotype on the microbiome. *Microbiome*, 6(1), p.31.

Delwiche, K.B. et al., 2021. FLUXNET-CH_4: a global, multi-ecosystem dataset and analysis of methane seasonality from freshwater wetlands. *Earth system science data*, 13(7), pp.3607–3689.

Douglas, G.M. et al., 2020. PICRUSt2 for prediction of metagenome functions. *Nature biotechnology*, 38(6), pp.685–688.

Epron, D. et al., 2022. Variability in stem methane emissions and wood methane production of different tree species in a cold temperate mountain forest. *Ecosystems (New York, N.Y.)*, 26(4), pp.784–799.

Evans, P.N. et al., 2015. Methane metabolism in the archaeal phylum Bathyarchaeota revealed by genome-centric metagenomics. *Science*, 350(6259), pp.434–438.

Feng, H. et al., 2022. Methane emissions may be driven by hydrogenotrophic methanogens inhabiting the stem tissues of poplar. *The New phytologist*, 233(1), pp.182–193.

Flanagan, L.B. et al., 2021. Multiple processes contribute to methane emission in a riparian cottonwood forest ecosystem. *The New phytologist*, 229(4), pp.1970–1982.

Forster, P. et al., 2021. The Earth's Energy Budget, Climate Feedbacks, and Climate Sensitivity. In V. Masson-Delmotte et al., eds. *Climate Change 2021: The Physical Science Basis. Contribution of Working Group I to the Sixth Assessment Report of the Intergovernmental Panel on Climate Change*. Cambridge, United Kingdom and New York, NY, USA: Cambridge University Press, pp. 923–1054.

Gauci, V. et al., 2024. Global atmospheric methane uptake by upland tree woody surfaces. *Nature*, 631(8022), pp.796–800.

Gauci, V., 2025. Tree methane exchange in a changing world. *Nature reviews. Earth & environment*, pp.1–13.

Gharechahi, J. et al., 2023. Lignocellulose degradation by rumen bacterial communities: New insights from metagenome analyses. *Environmental research*, 229(115925), p.115925.

Harada, M. et al., 2024. Ubiquity of methanogenic archaea in the trunk of coniferous and broadleaved tree species in a mountain forest. *Antonie van Leeuwenhoek*, 117(1), p.107.

Hettwer, C. et al., 2025. Methane flux from living tree stems in a northern conifer forest. *Biogeochemistry*, 168(4), pp.1–15.

Hüppi, R. et al., 2018. Restricting the nonlinearity parameter in soil greenhouse gas flux calculation for more reliable flux estimates. *PloS one*, 13(7), p.e0200876.

Hutchinson, G.L. & Mosier, A.R., 1981. Improved soil cover method for field measurement of nitrous oxide fluxes. *Soil Science Society of America journal. Soil Science Society of America*, 45(2), pp.311–316.

Jeffrey, L.C. et al., 2021. Bark-dwelling methanotrophic bacteria decrease methane emissions from trees. *Nature communications*, 12(1), p.2127.

Jeffrey, L.C. et al., 2023. Large methane emissions from tree stems complicate the wetland methane budget. *Journal of geophysical research. Biogeosciences*, 128(12). Available at: https://agupubs.onlinelibrary.wiley.com/doi/10.1029/2023JG007679.

Jeffrey, L.C. et al., 2024. Rapid bark-mediated tree stem methane transport occurs independently of the transpiration stream in Melaleuca quinquenervia. *The new phytologist*, 242(1), pp.49–60.

Jeffrey, L.C. et al., 2019. Rhizosphere to the atmosphere: contrasting methane pathways, fluxes, and geochemical drivers across the terrestrial–aquatic wetland boundary. *Biogeosciences* , 16(8), pp.1799–1815.

Jensen, K.F., 1967. Measuring oxygen and carbon dioxide in red oak trees. *Research Note NE-74. Upper Darby, PA: U.S. Department of Agriculture, Forest Service, Northeastern Forest Experiment Station. 4p.*, 74. Available at: https://research.fs.usda.gov/treesearch/download/10474.pdf [Accessed February 13, 2025].

Kaminsky, R.A. et al., 2023. Rumen *Lachnospiraceae* isolate NK3A20 exhibits metabolic flexibility in response to substrate and coculture with a methanogen. *Applied and Environmental Microbiology*, 89(10), pp.e00634–23.

Keiluweit, M. et al., 2018. Anoxic microsites in upland soils dominantly controlled by clay content. *Soil biology & biochemistry*, 118, pp.42–50.

Kolb, S. et al., 2003. Quantitative Detection of Methanotrophs in Soil by Novel pmoA-Targeted Real-Time PCR Assays. *Applied and environmental microbiology*, 69(5), pp.2423–2429.

Lacroix, E.M. et al., 2023. Consider the anoxic microsite: Acknowledging and appreciating spatiotemporal redox heterogeneity in soils and sediments. *ACS earth & space chemistry*, 7(9), pp.1592–1609.

Le Mer, J. & Roger, P., 2001. Production, oxidation, emission and consumption of methane by soils: A review. *European journal of soil biology*, 37(1), pp.25–50.

Leung, P.M. et al., 2024. Wetland tree barks are dynamic hotspots for microbial trace gas cycling. *bioRxiv*, p.2024.07.02.601631. Available at: https://www.biorxiv.org/content/10.1101/2024.07.02.601631v1.abstract [Accessed August 13, 2024].

Liu, C. et al., 2021. microeco: an R package for data mining in microbial community ecology. *FEMS microbiology ecology*, 97(2). Available at: http://dx.doi.org/10.1093/femsec/fiaa255.

1061 Louca, S., Parfrey, L.W. & Doebeli, M., 2016. Decoupling function and taxonomy in the global
1062 ocean microbiome. *Science*, 353(6305), pp.1272–1277.
1063 Luesken, F.A. et al., 2011. pmoA Primers for detection of anaerobic methanotrophs. *Applied and*
1064 *environmental microbiology*, 77(11), pp.3877–3880.
1065 Machacova, K. et al., 2023. Methane emission from stems of European beech (Fagus sylvatica)
1066 offsets as much as half of methane oxidation in soil. *The new phytologist*, 238(2), pp.584–
1067 597.
1068 McDonald, I.R., Kenna, E.M. & Murrell, J.C., 1995. Detection of methanotrophic bacteria in
1069 environmental samples with the PCR. *Applied and environmental microbiology*, 61(1),
1070 pp.116–121.
1071 McDonald, I.R. & Murrell, J.C., 1997. The particulate methane monooxygenase gene pmoA and
1072 its use as a functional gene probe for methanotrophs. *FEMS microbiology letters*, 156(2),
1073 pp.205–210.
1074 McMurdie, P.J. & Holmes, S., 2013. phyloseq: An R Package for Reproducible Interactive
1075 Analysis and Graphics of Microbiome Census Data M. Watson, ed. *PloS one*, 8(4),
1076 p.e61217.
1077 Megonigal, J.P., Brewer, P.E. & Knee, K.L., 2020. Radon as a natural tracer of gas transport
1078 through trees. *The new phytologist*, 225(4), pp.1470–1475.
1079 Mieszkin, S. et al., 2021. Oak decaying wood harbors taxonomically and functionally different
1080 bacterial communities in sapwood and heartwood. *Soil biology & biochemistry*, 155,
1081 p.108160.
1082 Mochidome, T. et al., 2025. Local methanogenesis drives significant methane emissions from
1083 upper tree trunks in a cool-temperate upland forest. *The new phytologist*. Available at:
1084 http://dx.doi.org/10.1111/nph.70331 [Accessed July 29, 2025].
1085 Moisan, M.-A. et al., 2025. Tissue humidity and pH as important species traits regulating tree
1086 methane emissions in floodplain wetland forests. *The new phytologist*, (nph.70543).
1087 Available at: http://dx.doi.org/10.1111/nph.70543 [Accessed September 9, 2025].
1088 Moll, J. et al., 2018. Bacteria inhabiting deadwood of 13 tree species are heterogeneously
1089 distributed between sapwood and heartwood. *Environmental microbiology*, 20(10),
1090 pp.3744–3756.
1091 Morotomi, M., Nagai, F. & Watanabe, Y., 2012. Description of Christensenella minuta gen.
1092 nov., sp. nov., isolated from human faeces, which forms a distinct branch in the order
1093 Clostridiales, and proposal of Christensenellaceae fam. nov. *International journal of*
1094 *systematic and evolutionary microbiology*, 62(Pt 1), pp.144–149.
1095 Nouchi, I., Mariko, S. & Aoki, K., 1990. Mechanism of methane transport from the rhizosphere
1096 to the atmosphere through rice plants. *Plant physiology*, 94(1), pp.59–66.
1097 Ntaikou, I. et al., 2008. Hydrogen production from sugars and sweet sorghum biomass using
1098 Ruminococcus albus. *International journal of hydrogen energy*, 33(4), pp.1153–1163.
1099 Nunan, N., Schmidt, H. & Raynaud, X., 2020. The ecology of heterogeneity: soil bacterial
1100 communities and C dynamics. *Philosophical transactions of the Royal Society of London.*

Series B, Biological sciences, 375(1798), p.20190249.

Pangala, S.R. et al., 2017. Large emissions from floodplain trees close the Amazon methane budget. *Nature*, 552(7684), pp.230–234.

Pangala, S.R. et al., 2015. The contribution of trees to ecosystem methane emissions in a temperate forested wetland. *Global change biology*, 21(7), pp.2642–2654.

Pangala, S.R. et al., 2013. Trees are major conduits for methane egress from tropical forested wetlands. *The New phytologist*, 197(2), pp.524–531.

Parolari, A.J., Sizemore, J. & Katul, G.G., 2021. Multiscale legacy responses of soil gas concentrations to soil moisture and temperature fluctuations. *Journal of geophysical research. Biogeosciences*, 126(2). Available at: http://dx.doi.org/10.1029/2020jg005865.

Pitz, S.L. et al., 2018. Methane fluxes from tree stems and soils along a habitat gradient. *Biogeochemistry*, 137(3), pp.307–320.

Pitz, S. & Megonigal, J.P., 2017. Temperate forest methane sink diminished by tree emissions. *The New phytologist*, 214(4), pp.1432–1439.

Polussa, A. et al., 2021. Scale dependence in functional equivalence and difference in the soil microbiome. *Soil biology & biochemistry*, 163(108451), p.108451.

Putkinen, A. et al., 2021. New insight to the role of microbes in the methane exchange in trees: evidence from metagenomic sequencing. *The New phytologist*, 231(2), pp.524–536.

Quast, C. et al., 2013. The SILVA ribosomal RNA gene database project: improved data processing and web-based tools. *Nucleic acids research*, 41(Database issue), pp.D590–6.

Rheault, K., Christiansen, J.R. & Larsen, K.S., 2024. goFlux: A user-friendly way to calculate GHG fluxes yourself, regardless of user experience. *Journal of open source software*, 9(96), p.6393.

Rocca, J.D. et al., 2015. Relationships between protein-encoding gene abundance and corresponding process are commonly assumed yet rarely observed. *The ISME journal*, 9(8), pp.1693–1699.

Ruaud, A. et al., 2020. Syntrophy via interspecies H_2 transfer between *Christensenella* and *Methanobrevibacter* underlies their global cooccurrence in the human gut. *mBio*, 11(1). Available at: http://dx.doi.org/10.1128/mbio.03235-19.

Schimel, J.P., 1995. Plant transport and methane production as controls on methane flux from arctic wet meadow tundra. *Biogeochemistry*, 28(3), pp.183–200.

Schink, B. & Ward, J.C., 1984. Microaerobic and Anaerobic Bacterial Activities Involved in Formation of Wetwood and Discoloured Wood. *IAWA journal / International Association of Wood Anatomists*, 5(2), pp.105–109.

Shigo, A.L. & Hillis, W.E., 1973. Heartwood, Discolored Wood, and Microorganisms in Living Trees. *Annual review of phytopathology*, 11(1), pp.197–222.

Siegenthaler, A. et al., 2016. Technical Note: Semi-rigid chambers for methane gas flux measurements on tree stems. *Biogeosciences* , 13(4), pp.1197–1207.

Sorz, J. & Hietz, P., 2006. Gas diffusion through wood: implications for oxygen supply. *Trees*, 20(1), pp.34–41.

Steinberg, L.M. & Regan, J.M., 2009. mcrA-targeted real-time quantitative PCR method to examine methanogen communities. *Applied and environmental microbiology*, 75(13), pp.4435–4442.

Uroz, S. et al., 2016. Ecology of the forest microbiome: Highlights of temperate and boreal ecosystems. *Soil biology & biochemistry*, 103, pp.471–488.

Waring, B.G. et al., 2016. Scale-dependent variation in nitrogen cycling and soil fungal communities along gradients of forest composition and age in regenerating tropical dry forests. *The new phytologist*, 209(2), pp.845–854.

Warner, D.L. et al., 2017. Carbon Dioxide and Methane Fluxes From Tree Stems, Coarse Woody Debris, and Soils in an Upland Temperate Forest. *Ecosystems* , 20(6), pp.1205–1216.

Watson, A. et al., 1997. Oxidation of methane in peat: Kinetics of CH4 and O2 removal and the role of plant roots. *Soil biology & biochemistry*, 29(8), pp.1257–1267.

Weber, N. et al., 2018. Nephele: a cloud platform for simplified, standardized and reproducible microbiome data analysis B. Berger, ed. *Bioinformatics* , 34(8), pp.1411–1413.

Weimer, P.J., 2022. Degradation of cellulose and hemicellulose by ruminal microorganisms. *Microorganisms*, 10(12), p.2345.

Wood, S.A. et al., 2023. Mitigating near-term climate change. *Environmental research letters*, 18(10), p.101002.

Wright, M.N. & Ziegler, A., 2017. ranger: A Fast Implementation of Random Forests for High Dimensional Data in C++ and R. *Journal of Statistical Software*, 77(1), pp.1–17. Available at: http://dx.doi.org/10.18637/jss.v077.i01.

Yip, D.Z. et al., 2019. Methanogenic Archaea dominate mature heartwood habitats of Eastern Cottonwood (Populus deltoides). *The New phytologist*, 222(1), pp.115–121.

Zaplana, T., Miele, S. & Tolonen, A.C., 2024. Lachnospiraceae are emerging industrial biocatalysts and biotherapeutics. *Frontiers in Bioengineering and Biotechnology*, 11 - 2023. Available at: http://dx.doi.org/10.3389/fbioe.2023.1324396.

Zausig, J., Stepniewski, W. & Horn, R., 1993. Oxygen concentration and redox potential gradients in unsaturated model soil aggregates. *Soil Science Society of America journal. Soil Science Society of America*, 57(4), pp.908–916.

Zeikus, J.G. & Henning, D.L., 1975. Methanobacterium arbophilicum sp.nov. An obligate anaerobe isolated from wetwood of living trees. *Antonie van Leeuwenhoek*, 41(4), pp.543–552.

Zeikus, J.G. & Ward, J.C., 1974. Methane Formation in Living Trees: A Microbial Origin. *Science*, 184(4142), pp.1181–1183.

Supporting Information

Supporting Information

Supporting Figures

- **Figure S1.** Mean relative abundances of potentially methanotrophic groups based on 16S rRNA sequencing across tree species and forest compartments
- **Figure S2.** Average relative abundance of different metabolisms per core type and per species (heartwood), as determined via FAPROTAX
- **Figure S3a.** Functional metabolic pathway analysis comparing inner and outer tree core segments based on PICRUSt2 predictions
- **Figure S3b.** Metabolic associations with methanotroph abundance
- **Figure S4.** Species-level variation in internal methane and oxygen concentrations from upland forest tree stems at Yale-Myers Forest
- **Figure S5.** Internal gas composition and methanogen abundance correlate with methane flux from upland forest tree stems
- **Figure S6.** Random forest model performance, feature importance, and response functions for tree stem and soil methane fluxes

Supplementary Methods and Results

S1. Tree-level prediction of methane flux

- **Figure S7.** Individual tree-level relationships between microbial gene abundance and methane flux controlling for species identity

S2. Species-level prediction of methane flux

- **Figure S8.** Species-level relationships between microbial gene abundance and methane flux in upland forest trees at Yale-Myers Forest
- **Figure S9.** Methanogen distribution in tree cross-sections and relationship with methane flux across species at Yale-Myers Forest

S3. Tissue-specific microbiomes of a single black oak

- **Figure S10.** Methanotroph distribution and pMMO:sMMO balance
- **Figure S11.** Independence of methanogen and methanotroph abundances at individual tree and species scales
- **Figure S12.** Methanogen and methanotroph abundance in a single black oak (*Quercus velutina*) tree across tissue types

Supplementary Field Methods

- **Figure S13.** Photo of representative semi-rigid chamber used 2020-2021
- **Figure S14.** Photo of representative rigid chamber used 2021-2023

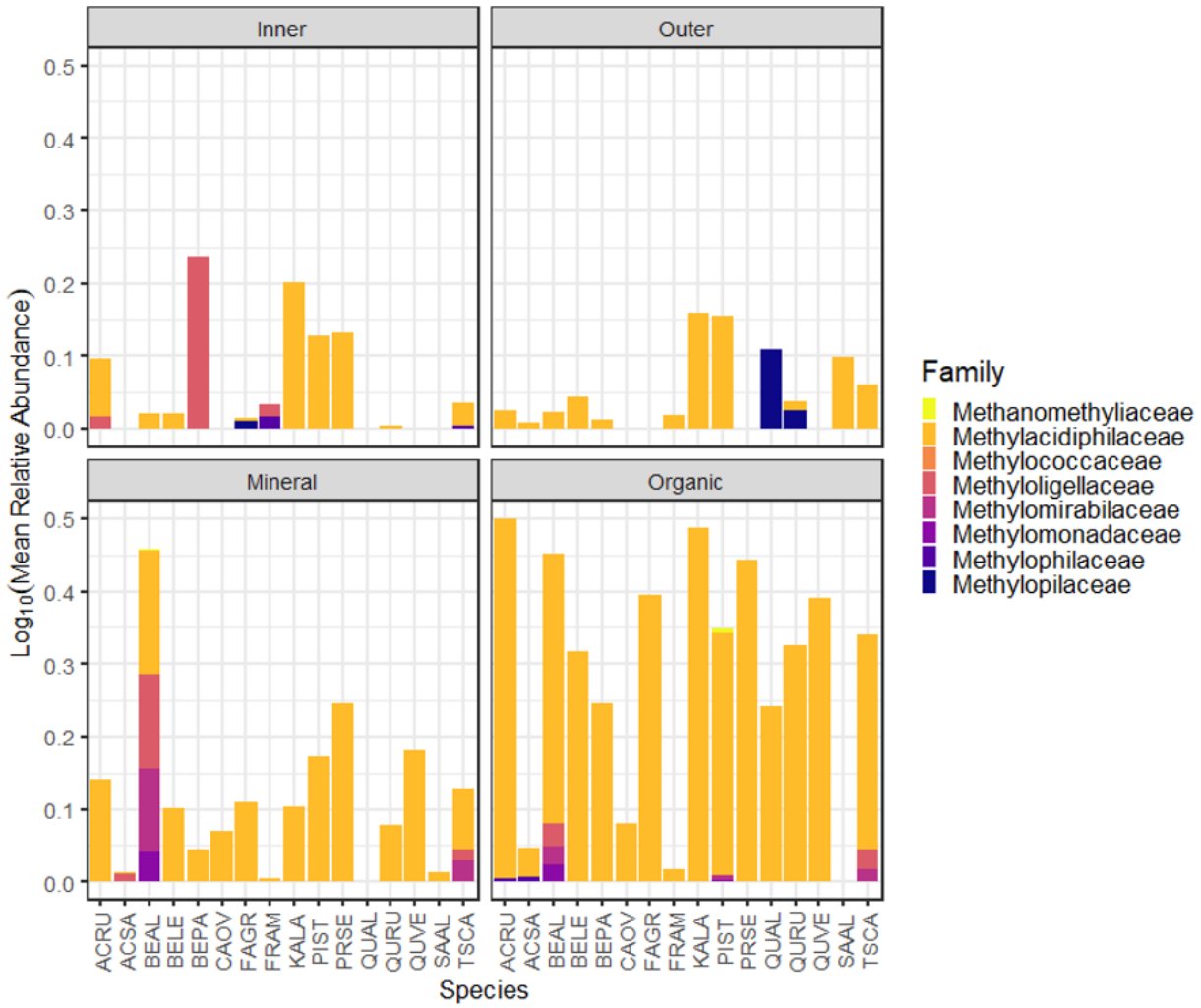

Figure S1: Mean relative abundances of potentially methanotrophic groups based on 16S rRNA sequencing across tree species and forest compartments. Bars show mean relative abundance (log_{10}-transformed) ± SE of bacterial families with putative or facultative methanotrophic capabilities across tree and soil samples at Yale-Myers Forest. Data shown for inner wood (heartwood-enriched), outer wood (sapwood-enriched), mineral soil, and organic soil samples. Species codes shown on x-axis (see main text for full species names). Families colored by taxonomy include taxa with confirmed or potential methane-oxidizing capabilities (Methylococcaceae, Methylocystaceae, Methylacidiphilaceae) as well as facultative methylotrophs that may metabolize methane under certain conditions (Methylophilaceae, Methylomonadaceae, and others). These taxa were most abundant in soil samples, particularly mineral and organic horizons, with lower abundances detected in wood tissues. This pattern contrasts with methanogens (Figure 5), which showed enrichment in heartwood relative to soils, reflecting the spatial segregation of methane production (anaerobic wood tissues) and consumption (aerobic soils and potentially outer wood layers) processes.

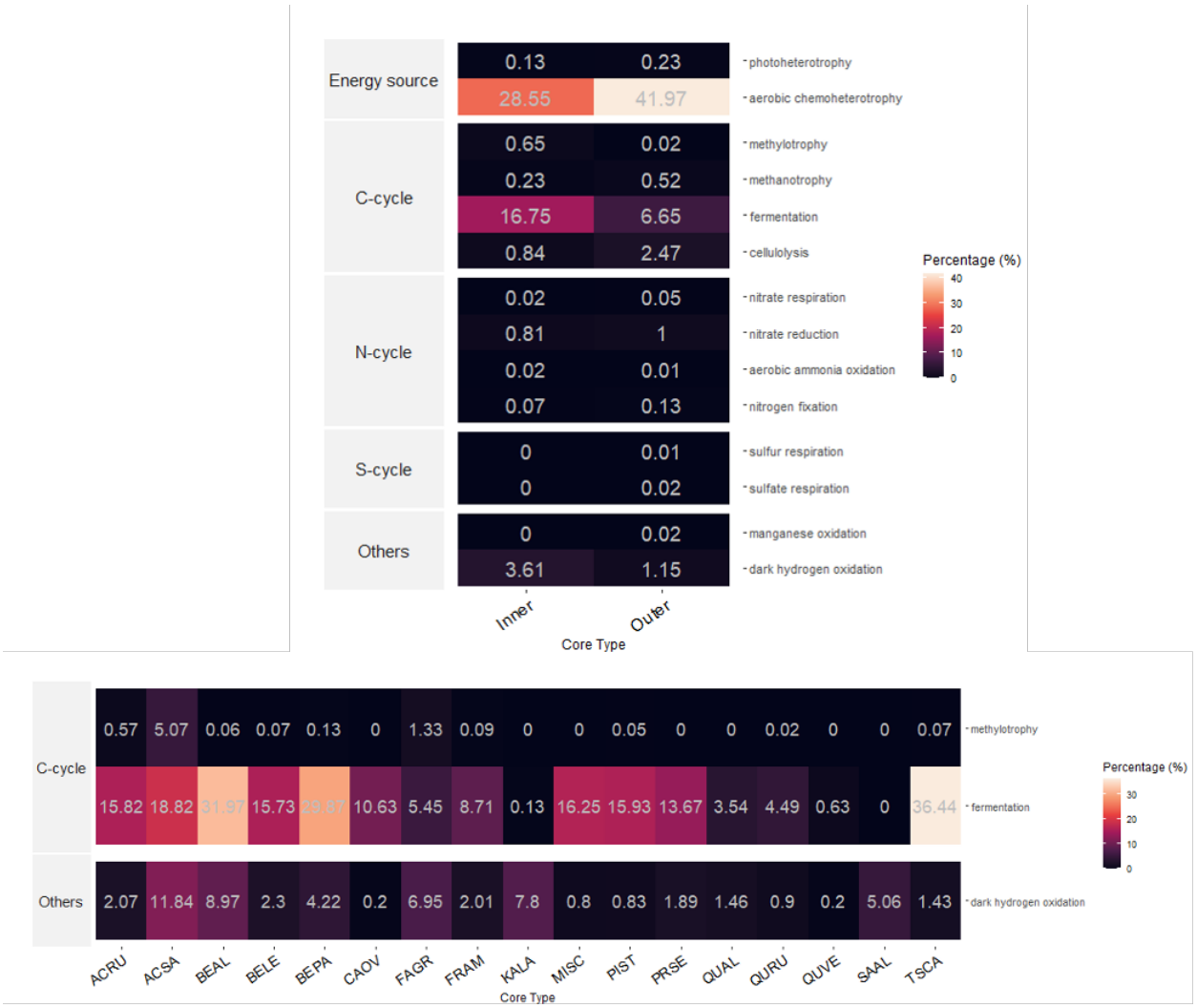

Figure S2: Average relative abundance of different metabolisms. a) Average relative abundance of different metabolisms per core type, as determined via FAPROTAX b) Average relative abundance of different metabolisms per species (heartwood), as determined via FAPROTAX

Figure S3a: Functional metabolic pathway analysis comparing inner and outer tree core segments based on PiCRUSt2 predictions. The heatmap shows the relative abundance of predicted metabolic pathways across tree core samples, organized by core type (inner in teal, outer in red) and methanogen abundance (log10 mcrA qPCR copies, green gradient at top). Each row represents a specific metabolic pathway, with pathway names listed on the y-axis. Color intensity indicates mean pathway abundance counts, with red showing higher abundance and blue showing lower abundance. The right color bar shows statistical significance (-logFDR), with green indicating significantly enriched pathways. Inner core samples show enrichment of anaerobic pathways including methanogenesis from H_2 and CO_2, methanogenesis from acetate, and various fermentation pathways. Outer core samples are enriched in aerobic pathways such as purine nucleotide degradation (aerobic), heme biosynthesis (aerobic), and assimilatory sulfur pathways, reflecting the redox gradient from anaerobic inner cores to more oxygenated outer cores.

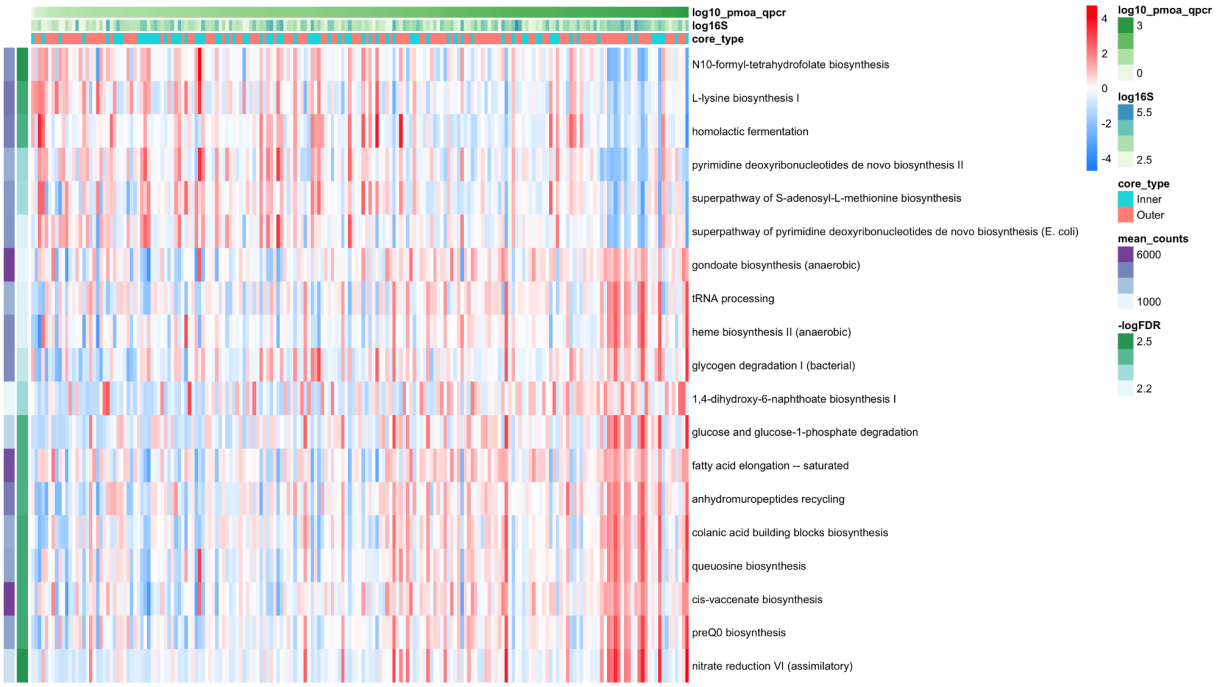

Figure S3b: Metabolic associations with methanotroph abundance. PICRUSt2 pathway predictions revealed distinct metabolic signatures associated with pmoA abundance across wood samples. Six pathways showed significant negative associations with pmoA abundance (FDR < 0.01), including N10-formyl-tetrahydrofolate biosynthesis, L-lysine biosynthesis, homolactic fermentation, pyrimidine deoxyribonucleotide biosynthesis, and S-adenosyl-L-methionine biosynthesis. The negative association with homolactic fermentation is consistent with methanotrophs being enriched in aerobic sites. Fourteen pathways showed significant positive associations with pmoA abundance (FDR < 0.01), including nitrate reduction, queuosine biosynthesis, multiple fatty acid biosynthesis pathways (cis-vaccenate, saturated fatty acid elongation), colanic acid building blocks, glucose degradation, heme biosynthesis, and tRNA processing. The association with nitrate reduction is consistent with the capacity of some methanotrophs to use nitrate as an alternative electron acceptor. As with associations for mcrA, these pathway associations represent predicted functions across the entire microbial community rather than methanotrophs (or methanogens, respectively) specifically, and caution is warranted in mechanistic interpretation. Note: While mmoX was detected by qPCR in 179 wood samples (comparable to pmoA detection in 189 samples), PICRUSt2 predicted mmoX presence in only 1 of 12,000+ ASVs in our 16S dataset. This poor reference database coverage precluded reliable pathway association analysis for mmoX. In contrast, pmoA and mcrA were predicted in 545 and 510 taxa respectively, enabling robust functional predictions for these markers.

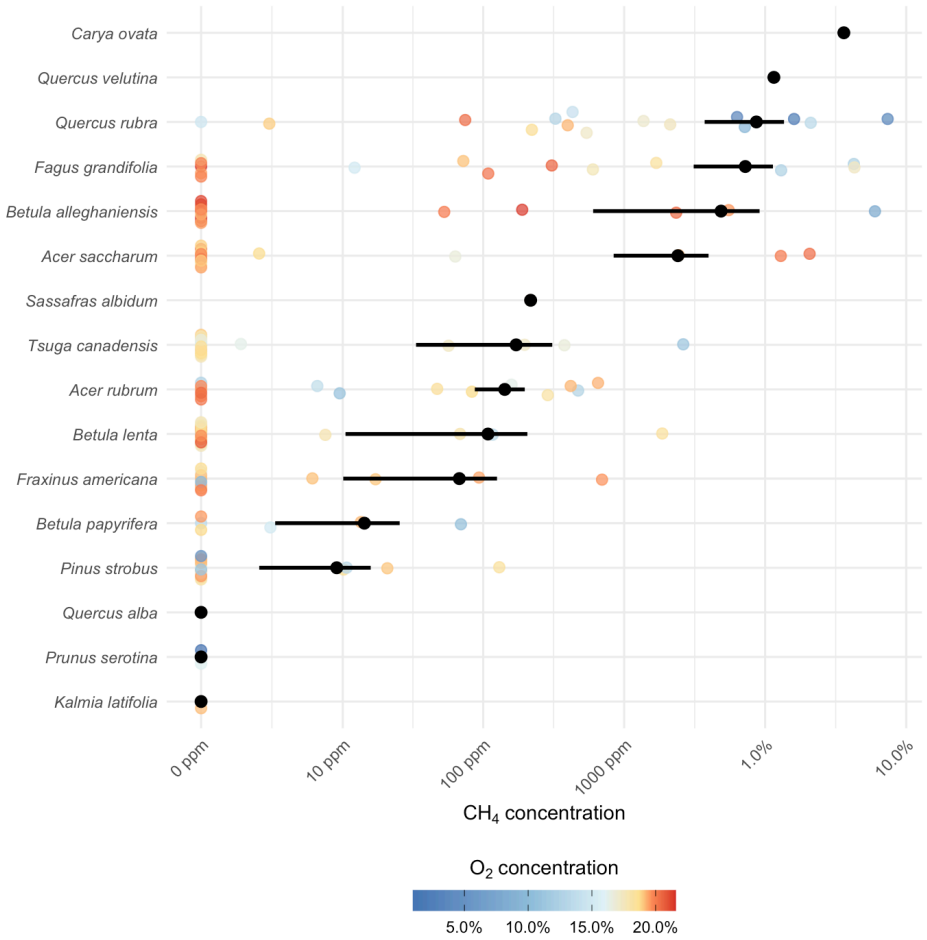

Figure S4. Species-level variation in internal methane and oxygen concentrations from upland forest tree stems at Yale-Myers Forest. Internal CH_4 concentration measurements at breast height (1.25 m) across 16 tree species, with individual trees shown as points distributed using a beeswarm layout to visualize sample density. Points colored by internal O_2 concentration, with cooler colors (blue) indicating lower oxygen and warmer colors (red) indicating higher oxygen availability. Black points with error bars show species mean ± standard error. Species ordered by mean CH_4 concentration from lowest (bottom) to highest (top). Y-axis displayed on pseudo-logarithmic scale to accommodate wide concentration ranges.

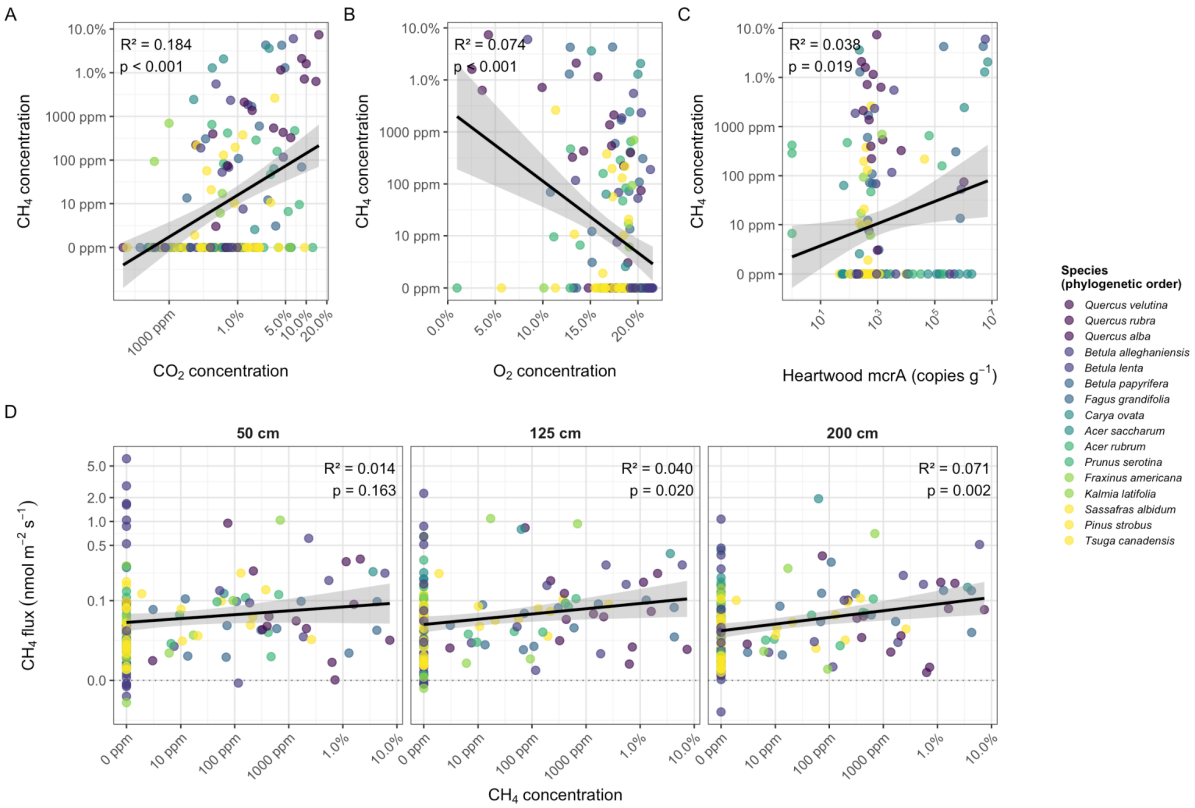

Figure S5. Internal gas composition and methanogen abundance correlate with methane flux from upland forest tree stems. (A) CH_4 flux versus internal CO_2 concentration. **(B)** CH_4 flux versus internal O_2 concentration. **(C)** CH_4 flux versus heartwood methanogen abundance (mcrA gene copies g^{-1}). **(D)** CH_4 flux versus internal CH_4 concentration at three stem heights (50, 125, 200 cm), with separate panels for each height. Points colored by tree species (legend, phylogenetic order). Axes displayed on pseudo-logarithmic scales (log_{10} for mcrA in panel C) to accommodate wide concentration ranges. Black lines show linear regression fits with 95% confidence intervals (shaded gray). Relationships between internal gas composition, methanogen colonization, and surface emissions suggest that methane production within tree tissues drives observed flux patterns.

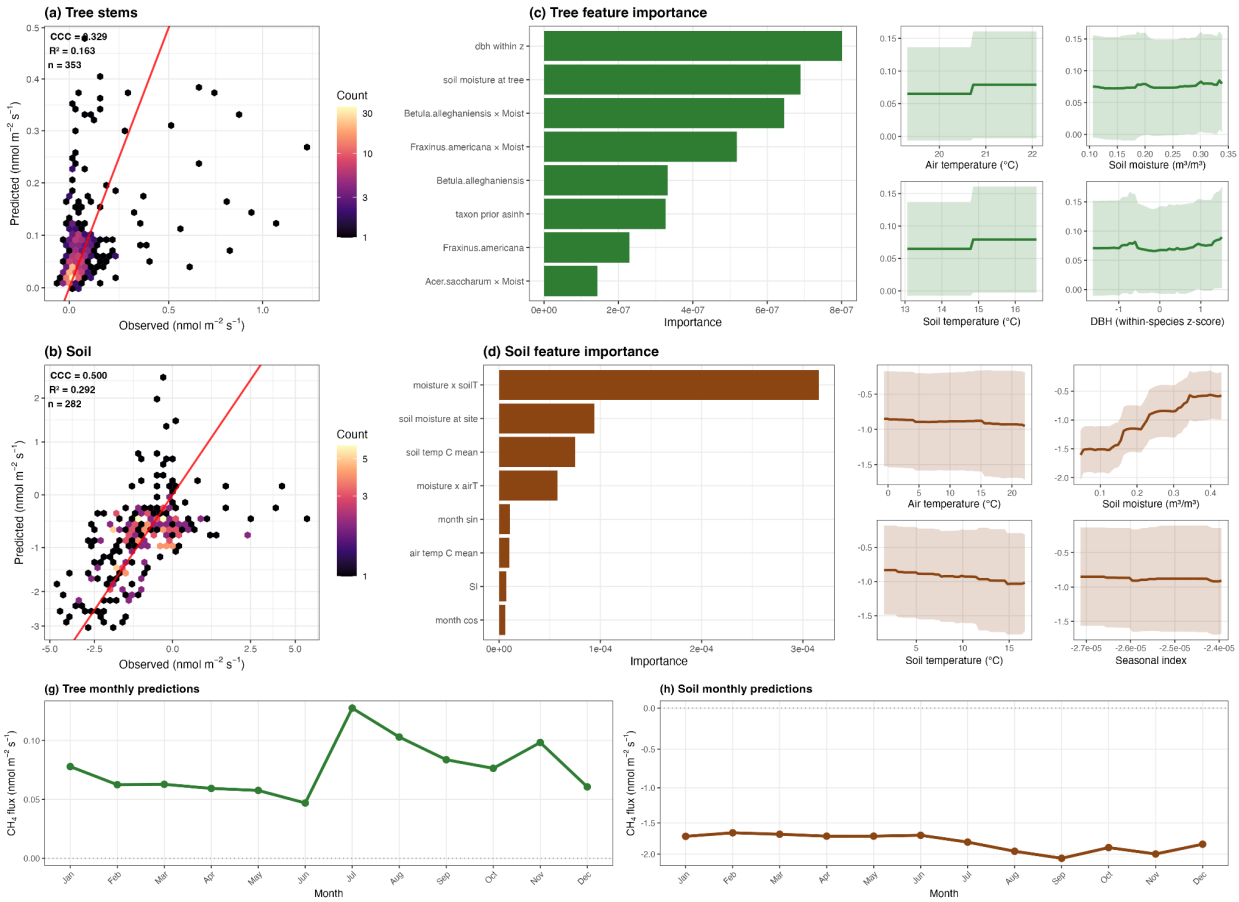

Figure S6: Random forest model performance, feature importance, and response functions for tree stem and soil methane fluxes. (a-b) Observed versus predicted CH_4 fluxes showing hexagonal binning to visualize point density. Model performance is evaluated using Lin's concordance correlation coefficient (CCC), which accounts for both precision and accuracy, and coefficient of determination (R^2). Red line indicates 1:1 agreement. Tree model: CCC = 0.329, R^2 = 0.163, n = 453; Soil model: CCC = 0.500, R^2 = 0.292, n = 262. (c-d) Feature importance rankings from random forest models showing the relative contribution of predictor variables to model performance. Tree model includes species identity, species×moisture interactions, and within-species standardized DBH (deconfounded for species identity). Soil model includes environmental drivers and their interactions. (e-f) Partial dependence plots showing the marginal effect of four key predictors on predicted CH_4 flux while averaging over all other variables. Shaded regions represent ±1 standard deviation across the prediction ensemble. Tree predictors: air temperature, soil moisture, soil temperature, and within-species DBH (z-score removes between-species size differences). Soil predictors: air temperature, soil moisture, soil temperature, and seasonal index (residual temporal variation). (g-h) Monthly predictions of mean CH_4 flux from tree stems and soil across the annual cycle, displayed on pseudo-log scale to accommodate the wide range of fluxes and negative values (soil uptake). Predictions integrate species composition, environmental conditions, and seasonal patterns from the random forest models.

Tree-Level Prediction of Methane Flux

Concentration-Based Linear Models

When tree genes were analyzed separately by tissue location (heartwood vs. sapwood, n = 121 trees with complete data), the full concentration model with species and six tissue-specific gene predictors explained 37.8% of variance (adjusted $R^2 = 0.253$, AIC = 16.1). In this model, only sapwood mmoX showed a significant relationship with flux ($\beta = -0.290$, SE = 0.105, $p = 0.007$, 95% CI [-0.498, -0.083]).

All other tissue-specific predictors were non-significant: heartwood mcrA ($\beta = -0.015$, SE = 0.022, $p = 0.481$, 95% CI [-0.058, 0.027]), sapwood mcrA ($\beta = -0.023$, SE = 0.022, $p = 0.278$, 95% CI [-0.066, 0.019]), heartwood mmoX ($\beta = -0.054$, SE = 0.043, $p = 0.214$, 95% CI [-0.139, 0.032]), heartwood pmoA ($\beta = -0.018$, SE = 0.031, $p = 0.554$, 95% CI [-0.080, 0.043]), and sapwood pmoA ($\beta = -0.050$, SE = 0.045, $p = 0.265$, 95% CI [-0.139, 0.039]). Type II ANOVA confirmed significant species effects ($F_{14,100} = 4.014$, $p = 1.83\times10^{-5}$) and sapwood mmoX effects ($F_{1,100} = 7.697$, $p = 0.007$), with all other gene terms non-significant (all $p > 0.21$).

Area-Weighted Linear Models

Linear mixed-effects models with species identity and area-weighted tree genes (n = 121 trees) revealed that tree mmoX was the strongest individual-tree predictor of methane flux. The best model included species and log-transformed tree mmoX ($R^2 = 0.356$, adjusted $R^2 = 0.264$, AIC = 10.3), with mmoX showing a significant negative relationship ($\beta = -0.356$, SE = 0.127, $p = 0.006$, 95% CI [-0.608, -0.104]). Type II ANOVA confirmed significant effects for both species ($F_{14,105} = 4.027$, $p = 1.54\times10^{-5}$) and log_tree_mmoX ($F_{1,105} = 7.848$, $p = 0.006$).

Models incorporating additional tree genes showed minimal improvement. Adding mcrA to the species + mmoX model increased R^2 marginally to 0.361 but worsened AIC (ΔAIC = 1.1). The species + mmoX + pmoA model similarly showed no improvement ($R^2 = 0.358$, ΔAIC = 1.6). The full model with all three genes explained 36.2% of variance (adjusted $R^2 = 0.256$, AIC = 13.2). Species identity alone explained 30.8% of variance (AIC = 17.0), indicating that mmoX provided significant additional predictive power beyond taxonomic effects alone.

The area-weighted approach explained slightly less variance than the concentration approach in full models (36.2% vs. 37.8%), though with fewer parameters (18 vs. 21).

Soil Gene Effects

Soil gene abundances provided no additional predictive power when added to tree-based models. Soil mcrA (tested on n = 74 trees) increased R^2 by only 0.001 ($p = 0.811$), soil pmoA (n = 107) by 0.003 ($p = 0.525$), and soil mmoX (n = 107) by <0.001 ($p = 0.796$).

Concentration-Based Random Forest Models

Random forest models substantially outperformed linear approaches at the tree level. The best-performing concentration-based model explained 49.9% of variance (MSE = 0.0664). Variable

importance rankings identified heartwood mcrA as the strongest predictor (%IncMSE = 7.04, IncNodePurity = 1.22), followed by sapwood methanotrophs (combined pmoA + mmoX; %IncMSE = 5.35, IncNodePurity = 0.84), sapwood mcrA (%IncMSE = 4.65, IncNodePurity = 0.54), soil mcrA (%IncMSE = 3.53, IncNodePurity = 0.28), sapwood pmoA (%IncMSE = 3.35, IncNodePurity = 0.63), and sapwood mmoX (%IncMSE = 3.22, IncNodePurity = 0.62). Another concentration-based variant with DBH normalization within species explained only 9.9% of variance (MSE = 0.0657).

Partial dependence analysis revealed non-linear relationships between predictors and flux, with most showing low linearity ($R^2 < 0.5$) indicating threshold or saturation effects. For these non-linear predictors, slopes are not reported as linear approximations are not meaningful. Heartwood mcrA showed total effect size of 0.117 across observed range (linearity $R^2 = 0.448$). Sapwood methanotrophs showed effect size of 0.075 (slope = -0.032 per unit, linearity $R^2 = 0.739$). Sapwood mcrA showed effect size of 0.087 (linearity $R^2 = 0.523$). Soil mcrA showed effect size of 0.079 (linearity $R^2 = 0.416$). Sapwood pmoA showed effect size of 0.061 (linearity $R^2 = 0.419$). Sapwood mmoX showed effect size of 0.079 (slope = -0.025 per unit, linearity $R^2 = 0.726$). Only sapwood methanotrophs and sapwood mmoX exceeded the linearity threshold ($R^2 > 0.7$), justifying reporting of linear slopes for these predictors.

Interaction analysis identified a single significant interaction between heartwood mcrA and sapwood methanotrophs (H-statistic = 0.508, interaction coefficient = 0.0053, $p = 0.0004$, $R^2 = 0.584$). Non-significant interactions were detected between sapwood methanotrophs and sapwood mcrA ($p = 0.218$) and heartwood mcrA and sapwood mcrA ($p = 0.599$).

Area-Weighted Random Forest Models

Area-weighted random forest models showed comparable performance to concentration-based approaches. The area-weighted model with DBH normalization explained 46.2% of variance (MSE = 0.0591), only 3.7 percentage points lower than the best concentration model. The basic area-weighted model without DBH normalization explained 36.7% (MSE = 0.0615), substantially outperforming the area-weighted linear models (36.2%). A simpler baseline random forest using only species and area-weighted genes explained only 12.8% of variance (MSE = 0.0646), indicating that environmental variables and non-linear modeling substantially improved predictions.

Both concentration-based and area-weighted random forest approaches yielded similar inference: (1) methanogen abundance (mcrA or heartwood mcrA) emerged as the top predictor in non-linear models despite being non-significant in linear models, (2) methanotroph genes showed negative relationships with flux, and (3) interactions between production and oxidation genes were detectable.

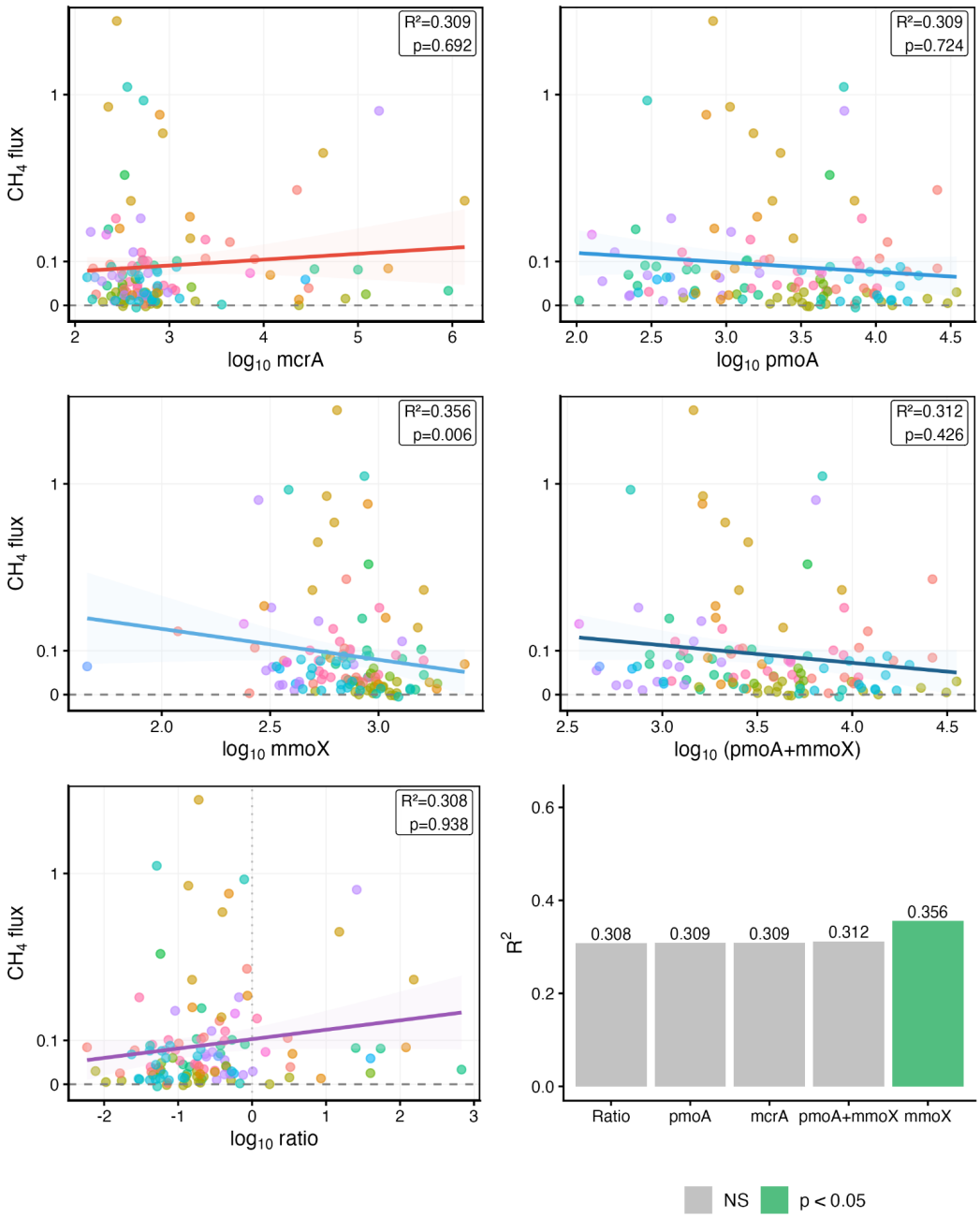

Figure S7: Individual tree-level relationships between microbial gene abundance and methane flux controlling for species identity. Data from trees with complete gene measurements (mcrA, pmoA, mmoX all detected). Top row: mcrA and pmoA. Middle row: mmoX and methanotrophs (pmoA+mmoX). Bottom row: methanogen:methanotroph ratio and model comparison. Linear mixed-effects models include species as covariate with model statistics (R^2 and p-value for gene predictor) displayed for each relationship.

Species-Level Prediction of Methane Flux

Concentration-Based Linear Models

At the species level using concentration-based measurements (n = 10 species with ≥5 observations each), heartwood mcrA showed the strongest correlation with flux ($R^2 = 0.611$, Pearson $r = 0.782$, $p = 0.008$). Other tissue-specific measurements showed weak or absent correlations: sapwood mcrA ($R^2 = 0.069$, $r = 0.263$, $p = 0.463$), heartwood mmoX ($R^2 = 0.001$, $r = -0.023$, $p = 0.950$), and sapwood mmoX ($R^2 = 0.000$, $r = -0.017$, $p = 0.963$). A combined model with both sapwood and heartwood mmoX explained only 0.1% of variance ($p = 0.997$).

Area-Weighted Linear Models

Aggregating area-weighted data to species level revealed correlations absent at individual tree level. Median area-weighted mcrA abundance showed a positive correlation with median flux. Log-transformed data yielded $R^2 = 0.403$ (Pearson $r = 0.635$, $p = 0.049$). Area-weighted mmoX showed a weak negative correlation ($R^2 = 0.068$, Pearson $r = -0.261$, $p = 0.467$).

Analysis of methanogen:methanotroph ratios showed stronger correlations than either gene alone. The ratio explained 53.8% of variance in species-level flux (Pearson $r = 0.711$ on log-transformed ratio, $p = 0.016$; Spearman $\rho = 0.661$, $p = 0.044$; Kendall $\tau = 0.511$, $p = 0.047$). Linear regression of median flux on median log-ratio yielded $\beta = 0.039$ (SE = 0.014, $p = 0.021$, $R^2 = 0.506$, adjusted $R^2 = 0.445$).

Model comparison using AIC confirmed the ratio as the best species-level predictor among area-weighted approaches (AIC = -44.82), outperforming mcrA alone (AIC = -42.26, $R^2 = 0.403$, $p = 0.049$) and methanotrophs alone (AIC = -39.70, $R^2 = 0.229$, $p = 0.162$). When restricted to species with both gene measurements available, all three models used identical sample sizes (n = 10 species), confirming the ratio's superior explanatory power.

Comparison of Concentration and Area-Weighted Approaches at Species Level

Concentration-based heartwood mcrA outperformed area-weighted approaches at the species level ($R^2 = 0.611$ vs. 0.403 for area-weighted mcrA and 0.538 for ratio). However, the ratio approach captured the balance between production and consumption processes ($R^2 = 0.538$), which was not directly measurable with concentration data where heartwood and sapwood genes were analyzed separately rather than integrated across cross-sectional area.

Scale-Dependent Patterns

The dramatic improvement in correlations at species level compared to tree level demonstrates scale-dependent emergence of gene-flux relationships. Individual tree-level correlations between methanogen abundance and flux were weak ($R^2 < 0.1$ for both heartwood and sapwood in linear models). In contrast, species-level aggregation revealed strong correlations: heartwood mcrA from gene concentration data ($R^2 = 0.611$, $p = 0.008$), methanogen:methanotroph ratio from area-weighted data ($R^2 = 0.538$, $p = 0.016$), and area-weighted mcrA ($R^2 = 0.403$, $p = 0.049$). This pattern held across different gene measurements and normalization approaches, indicating that

species-level averaging reduces noise from within-tree spatial heterogeneity while preserving underlying biological signals.

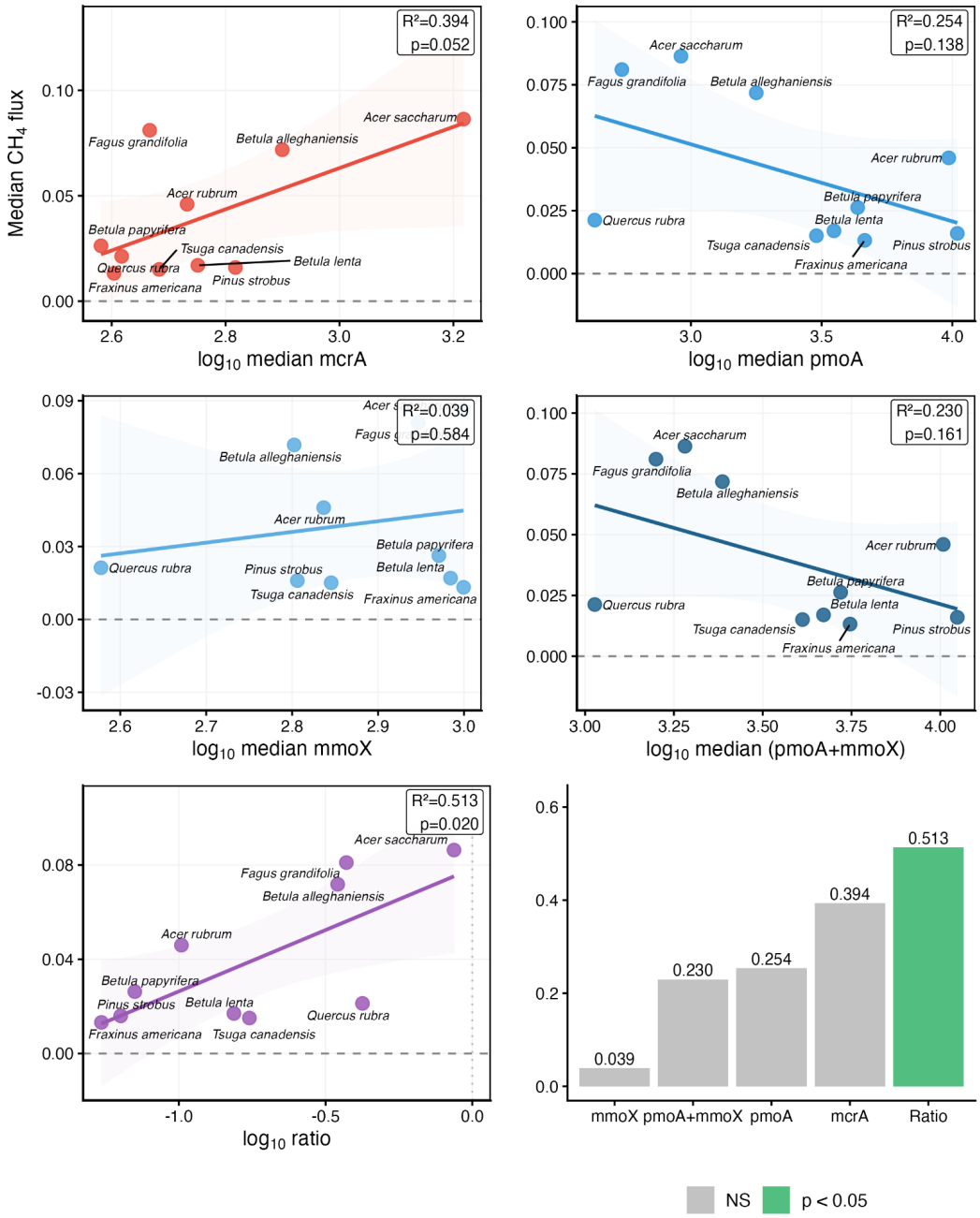

Figure S8: Species-level relationships between microbial gene abundance and methane flux in upland forest trees at Yale-Myers Forest. Data from trees with complete gene measurements (mcrA, pmoA, mmoX all detected, n=10 species with ≥5 trees each). Top row: mcrA and methanotrophs (pmoA+mmoX). Middle row: mmoX and pmoA. Bottom row: methanogen:methanotroph ratio and model comparison showing R^2 values for linear regressions using each gene predictor.

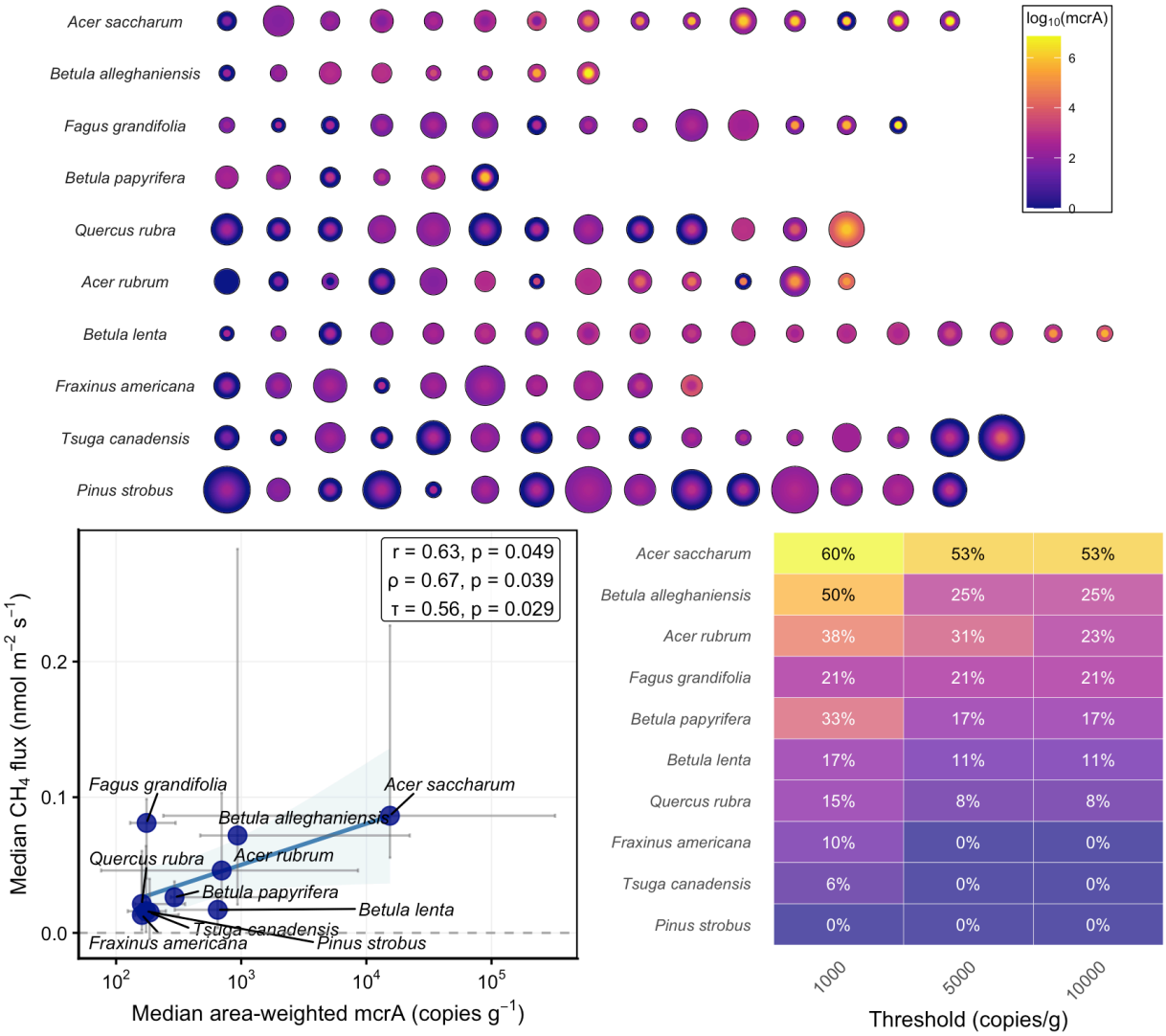

Figure S9. Methanogen distribution in tree cross-sections and relationship with methane flux across species at Yale-Myers Forest. (a) Interpolated radial distribution of mcrA gene abundance in tree stem cross-sections at breast height (1.25 m). Each circle represents an individual tree, organized by species (rows, n ≥ 3 trees per species) and individual trees within species (columns). Color intensity shows $\log_{10}$(mcrA copies g^{-1}) interpolated across a 0.5 cm resolution grid, with the color scale showing radial gradients from heartwood (center) to sapwood (periphery). Concentrations were modeled with a linear transition zone between inner wood (≤5 cm from pith) and outer wood (≤5 cm from bark) based on ddPCR quantification of mcrA genes from increment cores. Circle diameter is proportional to tree DBH. Sample size is slightly larger than in Fig. S8 because the dataset is not filtered for samples with methanotroph data in addition to methanogen data. (b) Correlation between median area-weighted mcrA abundance and median CH_4 flux aggregated by species. Area-weighted mcrA values integrate methanogen concentrations across stem cross-sectional areas, accounting for the relative contributions of heartwood and sapwood zones. Points represent species-level medians (n ≥ 5 trees per species for both measurements) with error bars showing interquartile ranges 25th-75th percentile). Blue line shows linear regression with 95% confidence interval (shaded). Statistical tests shown: Pearson r on $\log_{10}$-transformed data, Spearman ρ, and Kendall τ with p-values. (c) Proportion of trees exceeding methanogen abundance thresholds across species. Percentage of trees with area-weighted mcrA gene copies exceeding 1,000, 5,000, and 10,000 copies g^{-1}.

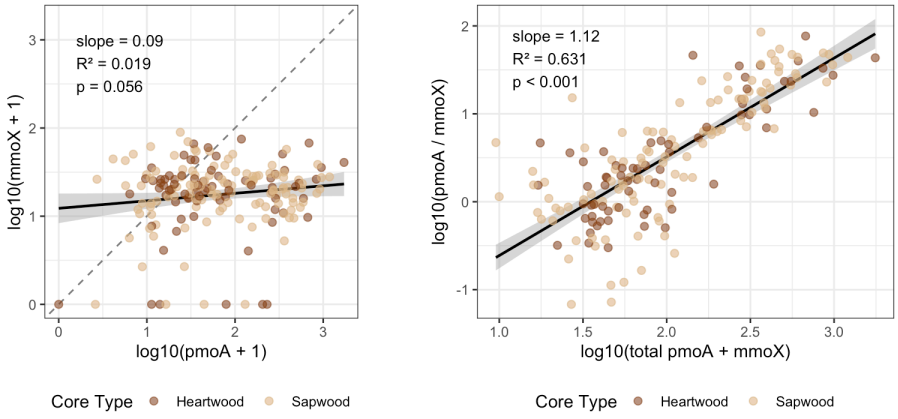

Figure S10: Methanotroph distribution and pMMO:sMMO balance. pmoA (particulate methane monooxygenase) was detected in 189 wood samples, while mmoX (soluble methane monooxygenase) was detected in 179 samples, with 94% co-occurrence in samples where either was present (Figure X). When both genes were detected, pmoA abundance was consistently higher than mmoX, with a median ratio of 2.9-fold (log10 ratio = 0.46 ± 0.69 SD). This ratio did not differ between heartwood and sapwood samples ($p = 0.37$) and was not correlated with methanogen abundance ($r = -0.03$, $p = 0.73$). However, the pmoA:mmoX ratio was strongly positively correlated with total methanotroph abundance ($r = 0.79$, $p < 0.001$), indicating that pMMO becomes increasingly dominant in samples with larger methanotroph populations (Figure X).

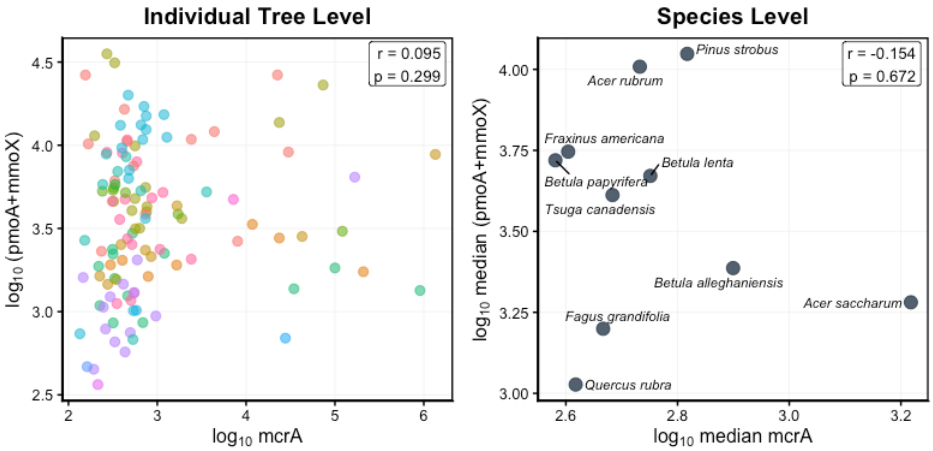

Figure S11. Independence of methanogen and methanotroph abundances at individual tree and species scales. Relationship between methanogens (mcrA) and methanotrophs (pmoA+mmoX) at individual tree level (left panel, n = 121 trees) and species level (right panel, n = 10 species). Individual tree data shows area-weighted gene abundances (log_{10}-transformed) with points colored by species. Species-level data shows median values with species labels in italics. Dashed diagonal line represents 1:1 relationship. At both scales, methanogens and methanotrophs showed no significant correlation (individual: $r = 0.095$, $p = 0.299$; species: $r = -0.154$, $p = 0.672$), indicating independent variation of these functional groups within tree stems.

Tissue-Specific Microbiomes of a Single Black Oak

Microbial community analysis of a single felled black oak (*Quercus velutina*) revealed distinct patterns of methanogen and methanotroph-related taxa across various tree tissues, including heartwood, sapwood, bark, branches, leaves, roots, and leaf litter. No methanogens were detected in soil samples from this tree, further supporting the hypothesis that methane emissions in upland trees are driven by internal methanogenic activity within tree tissues, rather than by soil-to-stem methane transport.

The only methanogen genus detected in the tree was *Methanobacterium* (family Methanobacteriaceae), which was found exclusively in heartwood and sapwood. This taxon was most abundant in heartwood, suggesting that internal anaerobic environments within tree tissues provide suitable conditions for methanogenesis. No methanogens were detected in oxygen-rich tissues such as bark, branches, or foliage, indicating that oxygen availability is a key limiting factor for methanogenic activity within trees.

In contrast, several methanotroph-related taxa were detected across various tree tissues, particularly in bark, sapwood, and leaf litter. These taxa were classified into three categories based on their methane-oxidation capabilities: known methanotrophs, potential methanotrophs, and methanotroph associates.

Known Methanotrophs: *Methylocella* (family Beijerinckiaceae) was detected in heartwood, sapwood, bark, and foliage. This genus is a facultative methanotroph capable of oxidizing both methane and multicarbon compounds, indicating that methane oxidation may occur within tree tissues. The widespread presence of Methylocella across different tissues suggests its potential role in reducing internal methane concentrations before methane is emitted from tree stems.

Potential Methanotrophs: *Methyloferula* (Beijerinckiaceae) was found in sapwood, bark, and leaf litter. This genus is considered an obligate methanotroph, utilizing soluble methane monooxygenase (sMMO) to oxidize methane. Its presence in tree-associated tissues further supports the possibility of methane oxidation occurring within the tree.

Methylorosula (Beijerinckiaceae) was detected in heartwood, sapwood, and leaf litter. While closely related to known methanotrophs, its capacity for methane oxidation has not been conclusively demonstrated. It is thus categorized as a potential methanotroph.

Methanotroph Associates: *Methylobacterium-Methylorubrum* and *Roseiarcus* (family *Beijerinckiaceae*) were detected across multiple tissues, including bark, sapwood, roots, and leaf litter. These genera are pink-pigmented facultative methylotrophs (PPFMs) that are known to utilize methanol and other single-carbon compounds, but they do not directly oxidize methane. Their presence in methane-rich environments suggests they may play a role in supporting methanotrophic activity or participating in co-metabolism with methanotrophs.

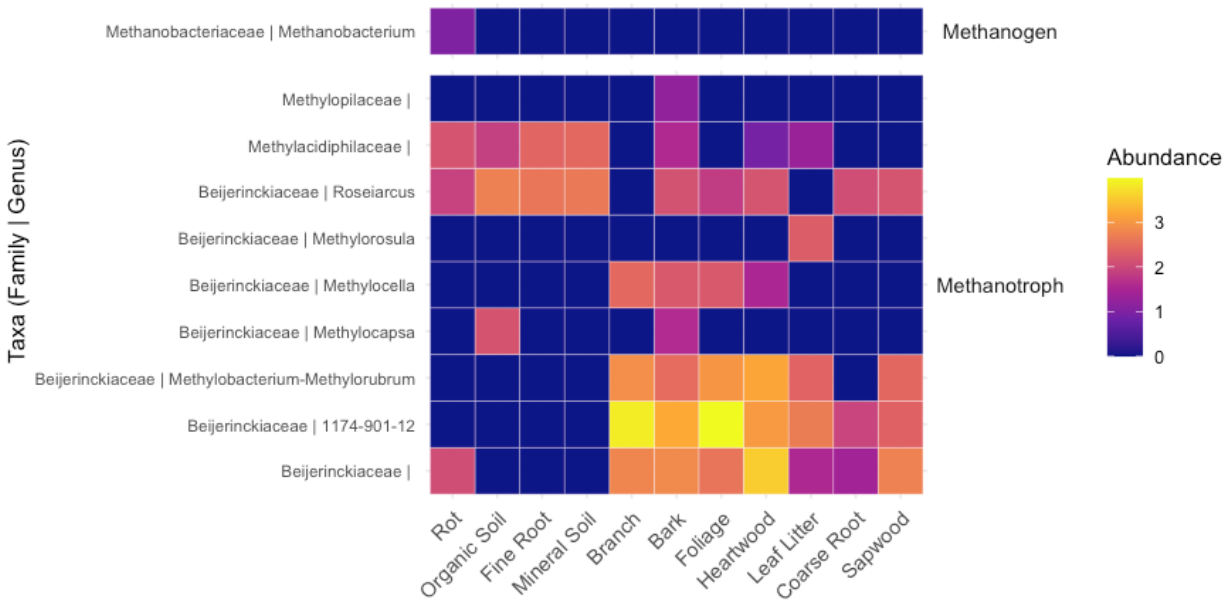

Figure S12: Methanogen and methanotroph abundance in a single black oak (Quercus velutina) tree across tissue types. Heatmap showing the distribution of methanogenic and methanotrophic taxa based on 16S rRNA gene sequencing across different tissues of a felled black oak at Yale-Myers Forest. Each column represents a different tissue type: heartwood, sapwood, bark, branches, leaves, roots, leaf litter, and surrounding soil. Rows show bacterial families grouped by functional role (methanogens vs. methanotrophs). Color intensity indicates $\log_{10}$-transformed relative abundance, with warmer colors (yellow-orange) showing higher abundance and cooler colors (blue-purple) showing lower abundance. Methanobacteriaceae (methanogens) were detected exclusively in a pocket of heart rot within the heartwood, demonstrating the localized nature of methanogenic colonization. Methanotrophic and methylotrophic taxa (Beijerinckiaceae families including Methylocella, Methyloferula, Methylorosula, and Methylobacterium-Methylorubrum) were distributed across various intern tissues.

Figure S13: Photo of representative semi-rigid chamber used 2020-2021.

Figure S14: Photo of representative rigid chamber used 2021-2023.